NHR-23 activity is necessary for developmental progression and apical extracellular matrix structure and function

Londen C. Johnson[1], An A. Vo[1], John C. Clancy[1], Joseph Aguilera[1], Max T. Levenson[1], Chloe Wohlenberg[1], Andreas Rechtsteiner[1], James Matthew Ragle[1], and Jordan D. Ward[1‡].

[1]Department of Molecular, Cell, and Developmental Biology, University of California-Santa Cruz, Santa Cruz, CA 95064, USA.

‡Author for correspondence.

Corresponding author email: jward2@ucsc.edu

Keywords: *C. elegans*, molting, NHR-23, nuclear hormone receptor, apical extracellular matrix, auxin-inducible degron

Running Title: NHR-23 in *C. elegans* molting

21 **Summary Statement**

22 This work provides insight into when and where the transcription factor NHR-23 acts to
23 promote apical extracellular matrix structure, function and remodeling in *C. elegans.*

24

25

SUMMARY STATEMENT

This work shows how a *C. elegans* transcription factor controls remodeling of the apical extracellular matrix during development and in which tissues it acts.

ABSTRACT

Nematode molting is a remarkable process where animals must repeatedly build a new apical extracellular matrix (aECM) beneath a previously-built aECM that is subsequently shed. The nuclear hormone receptor NHR-23/NR1F1 is an important regulator of *C. elegans* molting. NHR-23 expression oscillated in the epithelium, closely following the reported mRNA expression. Soma-specific NHR-23-depletion caused severe developmental delay and tissue-specific RNAi suggested that *nhr-23* acts primarily in seam cells. NHR-23 coordinates the expression of factors involved in molting, lipid transport/metabolism, and remodeling of the aECM. NHR-23 depletion caused dampened expression of a *nas-37* promoter reporter and a loss of reporter oscillation. The collagen ROL-6 and zona pellucida protein NOAH-1 displayed aberrant annular localization and severe disorganization over the seam cells following NHR-23 depletion. The expression of the adult cuticle-specific collagen BLI-1 was diminished and frequently found in patches. Consistent with these localization defects, the cuticle barrier was severely compromised. Together, this work provides insight into how NHR-23 acts in the seam and hypodermal cells to coordinate aECM regeneration during development.

INTRODUCTION

Molting is a critical developmental process required for the growth of all ecdysozoans, a clade comprising an estimated total of 4.5 million living species (Telford et al., 2008). Although specific to invertebrates, molting involves conserved processes such as apical extracellular matrix (aECM) remodeling, intracellular trafficking, and oscillatory gene expression (Lažetić and Fay, 2017). Molting is also a process of interest for developing new drugs against parasitic nematodes (Ghedin et al., 2007). Parasitic nematodes cause over a billion human infections each year and loss of livestock and crops (Ward, 2015b). However, very few drugs exist and resistance to those drugs is emerging rapidly (Ward, 2015b). While many genes involved in nematode molting have been identified in *C. elegans* (Frand et al., 2005), little is known about how their gene products are coordinated to promote aECM remodeling and the generation and release of a new cuticle.

Nematodes progress through four periodic larval stages (L1-L4), prior to becoming a reproductive adult (Brenner, 1974). The end of each larval stage is punctuated by a molt that involves trafficking and secretion of aECM components, assembly of a new aECM underneath the old cuticle, followed by separation of the cuticle from the underlying aECM (apolysis) and shedding of the old cuticle (ecdysis)(Lažetić and Fay, 2017). Apolysis coincides with a sleep-like behavior called lethargus (Singh and Sulston, 1978). The cuticle is a collagenous exoskeleton secreted by hypodermal and seam epithelial cells (Page and Johnstone, 2007). The outermost layer (glycocalyx) is rich in carbohydrates and mucins and thought to be secreted by the excretory gland cell (Nelson et al., 1983; Singh and Sulston, 1978). Beneath the glycocalyx is the glycolipid- and lipid-rich epicuticle which is postulated to function as a hydrophobic surface barrier (Blaxter, 1993; Blaxter et al., 1992). Underlying the epicuticle is a layer comprised mainly of cuticlin proteins. Between the epidermal membrane and the epicuticle are collagen rich layers, including a fluid-filled medial layer with collagen struts (Lažetić and Fay, 2017; Page and Johnstone, 2007). Sets of collagens oscillate in expression over the course of each molt and are classified into three groups based on temporal expression: early, intermediate, and late collagens (Johnstone and Barry, 1996; Page and Johnstone, 2007). While the specific localization of most collagens is unknown, collagens from the same group are

82 thought to be in the same layer. A transient structure, the sheath or pre-cuticle, is formed
83 during each larval stage and thought to pattern the cuticle (Cohen and Sundaram, 2020).
84 Many of the components of this pre-cuticle are related to mammalian matrix proteins. The
85 *C. elegans* pre-cuticle contains Zona Pellucida proteins, proteins related to small leucine-
86 rich proteoglycans, and lipid transporters in the lipocalin family (Cohen and Sundaram,
87 2020; Cohen et al., 2020; Forman-Rubinsky et al., 2017; Kelley et al., 2015; Sapio et al.,
88 2005; Vuong-Brender et al., 2017).
89
90 Nuclear hormone receptor (NHR) transcription factors are key regulators of molting in
91 insects and nematodes (King-Jones and Thummel, 2005; Taubert et al., 2011). NHRs are
92 characterized by a ligand-binding domain (LBD) which has the potential to bind small
93 molecules such as ligands and dietary-derived metabolites (Taubert et al., 2011). NHRs
94 have a canonical zinc finger DNA-binding domain (DBD) with an unstructured hinge
95 region between the DBD and LBD that is subject to post-translational regulation (Antebi,
96 2015; Campbell et al., 2008; Ward et al., 2013). A single, conserved nuclear hormone
97 receptor, NHR-23/NR1F1 (hereafter referred to as NHR-23), an ortholog of DHR3 in
98 insects and RORα in mammals, is a key regulator of *C. elegans* molting. *nhr-23* mutation
99 or inactivation by RNAi leads to embryonic lethality, larval arrest, ecdysis defects, and
100 morphology defects (Frand et al., 2005; Gissendanner et al., 2004; Kostrouchova et al.,
101 1998; Kostrouchova et al., 2001). *nhr-23* mRNA expression oscillates over the course of
102 each larval stage, peaking mid-larval stage and hitting a trough at the molt (Gissendanner
103 et al., 2004; Kostrouchova et al., 2001). Experiments with *nhr-23* mutants and RNAi have
104 demonstrated a role for NHR-23 in all four larval molts (Kostrouchova et al., 1998;
105 Kostrouchova et al., 2001). The NHR-23 insect ortholog (DHR3) is part of the molting
106 gene regulatory network (Lam et al., 1997; Ruaud et al., 2010) and the mammalian
107 ortholog (RORα) regulates circadian rhythms, lipid metabolism, and immunity (Jetten,
108 2009).
109
110 We found that NHR-23 protein oscillates and rapid NHR-23 depletion via an auxin-
111 inducible degron causes severe developmental delay. Analysis of NHR-23 target genes
112 suggests a role in coordinating aECM assembly, remodeling, and construction of specific

113 cuticular structures. NHR-23 depletion causes aberrant localization of the collagens ROL-
114 6 and BLI-1 and of the pre-cuticle factor NOAH-1. NHR-23 activity is necessary in seam
115 cells to promote molting and timely development. Our work provides an entry point into
116 understanding how NHR-23 coordinates the complex cell biology underpinning molting.
117

118 **RESULTS**

119 **NHR-23 oscillates during development**

120 Expression of *nhr-23* mRNA oscillates throughout each larval stage of the *C. elegans* life
121 cycle (Gissendanner et al., 2004; Hendriks et al., 2014; Kostrouchova et al., 2001;
122 Meeuse et al., 2020) reaching peak expression mid-intermolt and a trough prior to the
123 completion of the next molt (Fig. 1A). However, mRNA expression profiles do not always
124 match protein levels (de Sousa Abreu et al., 2009; Vogel and Marcotte, 2012). To
125 determine whether NHR-23 protein oscillates, we monitored the expression of the
126 endogenous NHR-23::GFP, over 28 hours. During L1, oscillating expression of NHR-
127 23::GFP was observed in the nuclei of seam and hypodermal cells (Fig. S1). Expression
128 of NHR-23 rises and falls prior to the completion of the 1st molt; this pattern is repeated
129 prior to the 2nd molt as well (Fig. 1B,C), similar to the reported mRNA expression
130 (Gissendanner et al., 2004; Kostrouchova et al., 2001). As GFP tags can affect the
131 expression or stability of proteins (Agbulut et al., 2006; Baens et al., 2006), we assayed
132 the expression of NHR-23 through western blotting time-courses using an *nhr-*
133 *23::AID*::3xFLAG* strain (Zhang et al., 2015). These experiments confirmed that NHR-
134 23::AID*::3xFLAG also oscillates (Fig. 1C), similar to our NHR-23::GFP imaging
135 experiments (Fig. 1B). We detected three distinct NHR-23 bands; the lowest band is
136 consistent with the size of NHR-23b/f (Fig. 1C,D, Fig. S2). The upper two bands are larger
137 than expected, which could reflect post-translational modification or that NHR-23 migrates
138 aberrantly during SDS-PAGE. All observed NHR-23 bands oscillate, though the lowest
139 band was expressed more strongly than the other bands (Fig. 1C).
140

141 **Distinct phenotypes caused by early or late NHR-23-depletion in L1 larvae**

142 Given that NHR-23 oscillates, we tested when NHR-23 was necessary for molting during
143 the L1 larval stage. We have previously shown that the auxin-inducible degron system

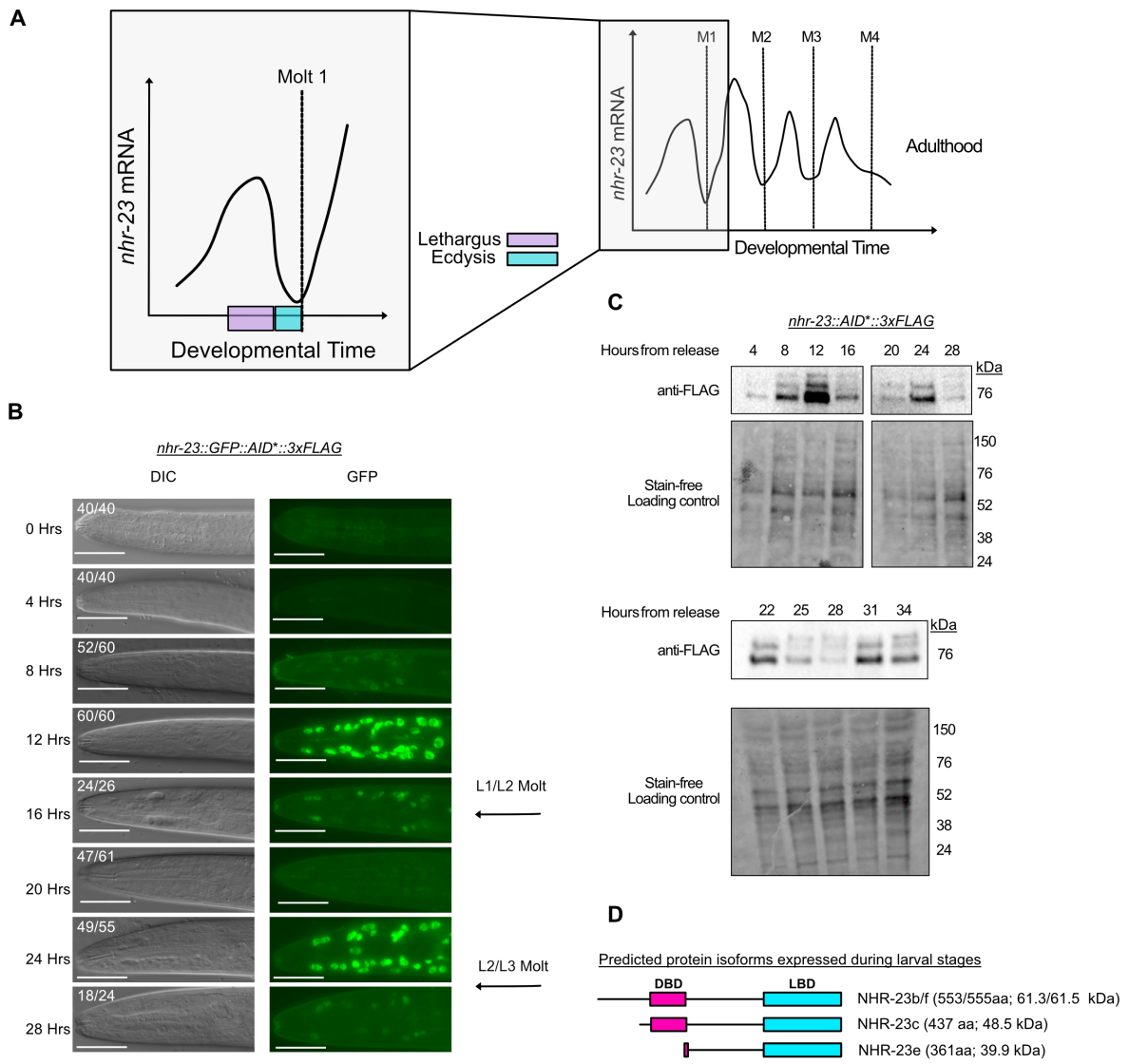

Fig. 1. NHR-23 protein oscillates during development. (A) A schematic of *nhr-23* mRNA expression across *C.* elegans larval development based on previous expression data (Gissendanner et al., 2004). (B) Representative images from a time course monitoring the expression of endogenous NHR-23 protein over the first 28 hours of larval development. The appropriate timing of the L1/L2 and L2/L3 molts is indicated. *nhr-23::GFP::AID*::3xFLAG* (B) and *nhr-23::AID*::3xFLAG* (C) are previously described endogenous knock-ins that produce C-terminal translational fusions to all known *nhr-23* isoforms (Ragle et al., 2020; Zhang et al., 2015). Two biological replicates were performed and the number of animals for which the image is representative at each timepoint is provided. Scale bars=20 µm. (C) Anti-FLAG immunoblot analysis of synchronized *nhr-23::AID**::3xFLAG animals monitoring the expression of NHR-23 3XFLAG across two time courses, 4-28 hours and 22-34 hours. Marker size (in kDa) is provided. Stain-free analysis, which visualizes total protein on the membrane, is provided as a loading control. The blots are representative of three experimental replicates. (D) Cartoons of predicted protein isoforms expressed during larval development based on Nanopore direct mRNA sequencing data (Roach et al., 2020). All of the predicted isoforms contain a Ligand Binding Domain (LBD) while only two of the three have a DNA Binding Domain (DBD). The predicted size of each isoform is listed to the right of the structure in amino acids (aa) and kDa. The AID*::3xFLAG fusion is predicted to add 9 kDa.

144

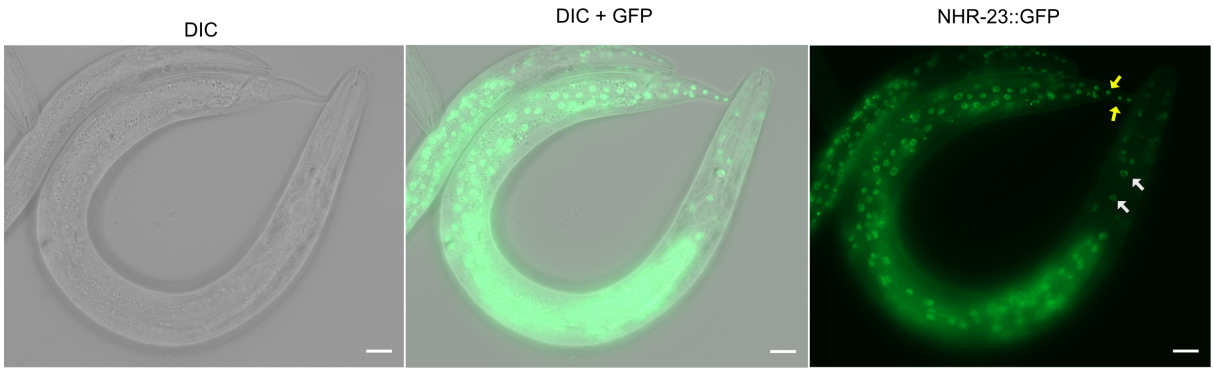

Fig. S1. NHR-23::GFP expression in hypodermal tissue. Representative image of NHR-23 expression in *nhr-23::GFP::AID*::3xFLAG; TIR-1* L4 animals. NHR-23 expression is seen in the hypodermis and developing germline, as described in Ragle et al. 2020. White arrows to seam cells expressing GFP and yellow arrows pointing to hyp cells expressing GFP.

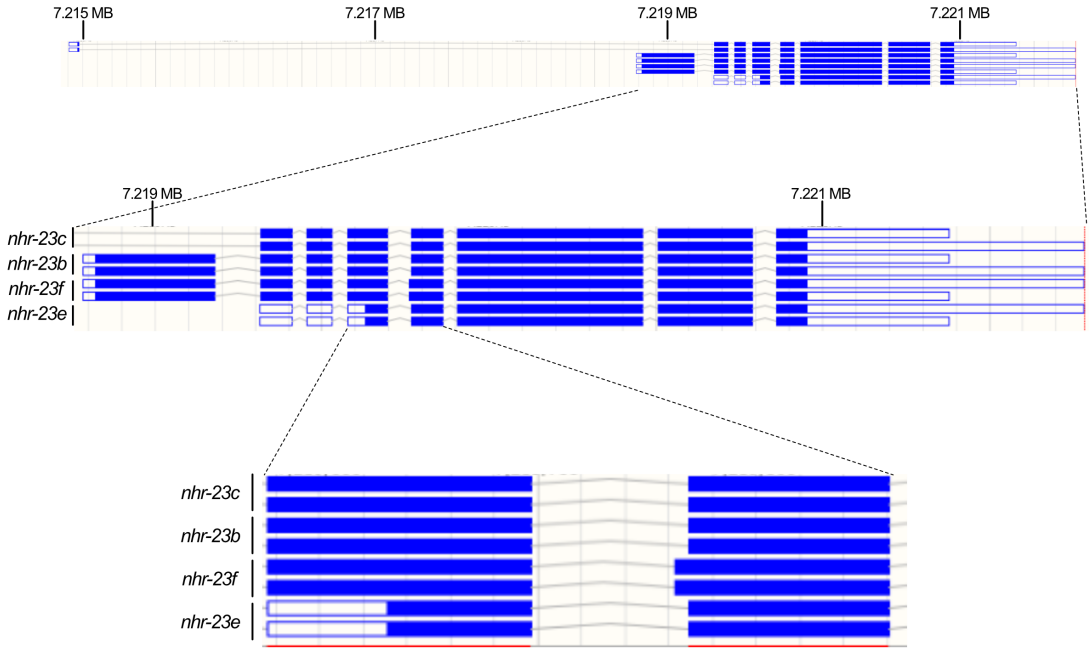

Fig. S2. *nhr-23* isoforms detected by Nanopore direct mRNA sequencing. Gene model diagrams of the *nhr-23* isoforms from the "observed isoforms" track on the ENSEMBL genome track. These are isoforms confirmed by direct mRNA sequencing (Roach et al., 2020). The top tracks are of the full *nhr-23* gene, including the *nhr-23c* isoforms, which contain a large first intron. The middle tracks are a zoomed in view starting at the *nhr-23b* transcription start site. The bottom tracks are further zoomed in to depict the alternative 3' splice site usage that generates *nhr-23b* and *nhr-23f*.

can rapidly deplete a nuclear hormone receptor (NHR-25), with almost complete depletion within 30 minutes (Zhang et al., 2015). In a pilot experiment, we consistently found weaker depletion phenotypes using an *nhr-23::GFP::AID*::3xFLAG* strain (Ragle et al., 2020)

compared to the *nhr-23::AID*::3xFLAG strain* (Zhang et al., 2015)(Table S1). We therefore transitioned to using the *nhr-23::AID*::3xFLAG* strain for all experiments involving phenotypic analysis. We first tested NHR-23::AID*::3xFLAG depletion kinetics and found robust depletion within 15 minutes after exposure to 4 mM auxin and levels remained low over the 16 hour time course (Fig. 2B).

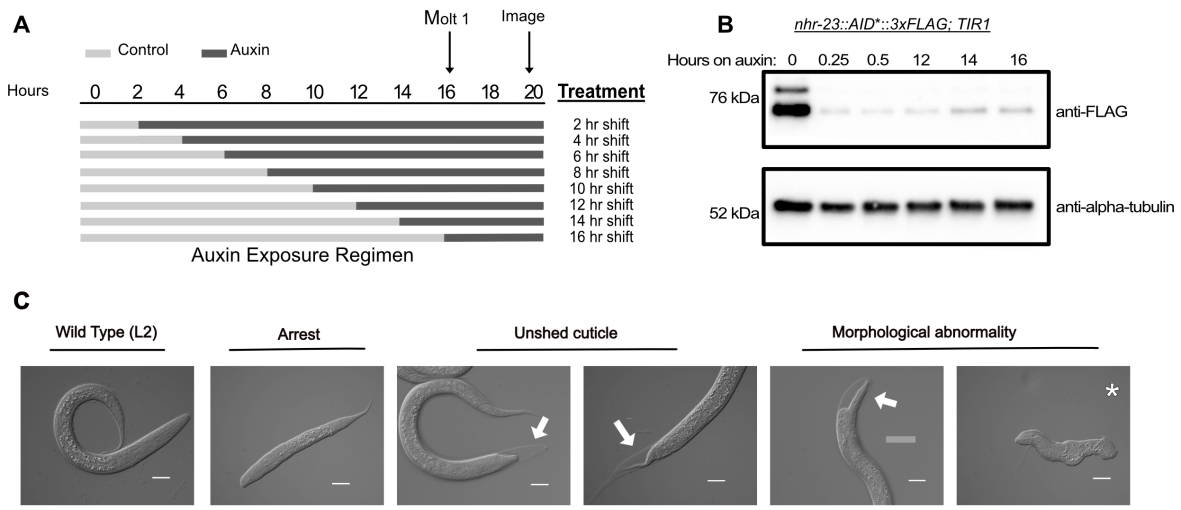

D

Phenotypic data for *nhr-23::AID*; *TIR1*

Shift Hour	(n)		% Unshed cuticle		% Morphological abnormality	
	nhr-23::AID; TIR1	*TIR1*	*nhr-23::AID; TIR1*	*TIR1*	*nhr-23::AID; TIR1*	*TIR1*
2	40	40	0	0	5	0
4	40	40	28	0	5	0
6	40	31	40	0	18	0
8	40	35	40	0	30	0
10	31	37	58	0	42	0
12	40	20	40	0	55	0
14	39	32	5	0	0	0
16	40	36	5	0	5	0

Fig. 2. Distinct phenotypes are observed when NHR-23 is depleted early or late in L1 larvae. (A) Schematic of the experimental set-up. Synchronized L1 larvae were grown on control media (light grey bands) and transferred to 4mM auxin (dark grey bands) every 2 hours. Animals remained on auxin until they were imaged at 20 hours post-release. (B) Anti-FLAG immunoblot to monitor NHR-23 depletion. Synchronized *nhr-23::AID*::3xFLAG; TIR1* and *TIR1* animals were grown on MYOB plates for 12 hours, which corresponded to the peak in L1 expression from Figure 1C. Animals were then shifted onto control or auxin plates and lysates were collected at the indicated time points. Marker size (in kDa) is provided. An anti-alpha-tubulin immunoblot is provided as a loading control. The blots are representative of three experimental replicates. (C) Representative images of phenotypes observed when *nhr-23::AID*::3xFLAG; TIR1* animals were exposed to auxin in the first larval stage. (D) Percent of animals of the indicated genotypes with unshed cuticles and morphological abnormalities following exposure to auxin. The number of animals scored (n) is provided.

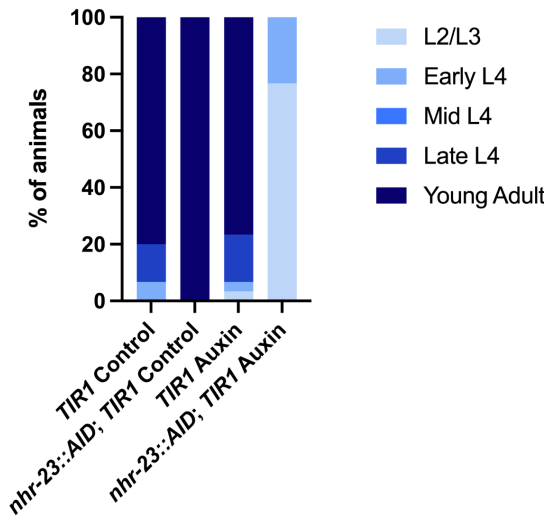

Fig. S3. Late depletion of NHR-23 in L1 leads to animals persisting in L2/L3. Synchronized *nhr-23::AID*::3xFLAG; TIR1* and *TIR1* animals were grown on MYOB media and shifted to auxin or control plates at 16 hours post release. 30 animals for each genotype and condition were staged 48 hours post shift based on vulval morphology (Mok et al., 2015). L4 larval stages were grouped as Early L4 (4.0-4.2), Mid L4 (4.3-4.5), and Late L4 (4.6-4.9). Percentage of animals in each stage is displayed for each genotype and condition. Data are from two experimental replicates and 30 animals were scored for each strain.

We performed timed depletion experiments in the L1 larval stage (Fig. 2A) using an *eft-3p::TIR1::mRuby2* control strain (henceforth referred to as *TIR1*) and a strain that permits somatic depletion of NHR-23 in the presence of auxin, (*eft-3p::TIR1::mRuby2; nhr-23::AID*::3xFLAG;* henceforth referred to as *nhr-23::AID*; *TIR1*). Synchronized L1s were shifted onto either 4 mM auxin or control plates every two hours (Figure 2A). Animals were scored for molting defects at 20 hours post-release. 100% of *TIR1* control animals shifted onto control or auxin plates successfully molted and transitioned into the second larval stage. *nhr-23::AID*; *TIR1* animals shifted onto control plates also reached the L2 stage, indicating that ethanol does not affect developmental timing in this context. In contrast, *nhr-23::AID*; *TIR1* animals shifted onto auxin displayed multiple phenotypes including molting defects, internal vacuoles, developmental abnormalities such as disrupted tails and viable animals with a squashed morphology ("splatter")(Fig. 2C). We then quantified the molting defects, scoring animals unable to shed their cuticles, or with morphological abnormalities (Fig. 2D). Vacuoles were observed in both the *TIR1* control and *nhr-23::AID; TIR1* strains. This could be a result of exposure to auxin or possibly an effect of the imaging process. We did not pursue the vacuole phenotype further. The percentage of *nhr-23::AID*; *TIR1* animals with unshed cuticles was low (5%) when animals were shifted to auxin 2 hours post-release (Fig. 2D). This percentage increased the later animals were shifted to auxin, reaching a maximum of 58% when animals were shifted 12 hours post-release (Fig. 2D). The majority of *NHR-23::AID; TIR1* animals shifted on to auxin at the 14 and 16 hour time points appeared wild

184 type (Fig. 2D). *TIR1* and *nhr-23::AID; TIR1* animals grown on control plates developed
185 normally with no arrest or morphological defects (n=35 for each strain). We repeated the
186 16 hour shift experiment and scored animals 48 hours later. Based on size, gonadal
187 morphology, and vulval morphology, animals were L2 and L3 larvae (Figure S3). These
188 data suggest that NHR-23 is necessary during the 4-12 hour post-release window to
189 promote the L1 molt, then is dispensable during the 14-16 hour post-release window.
190

191 **NHR-23 depletion causes severe developmental delay**

192 *nhr-23::AID*; *TIR1* animals exposed to auxin at hours 2 and 4 appeared smaller than
193 control animals and had fewer molting defects than animals shifted onto auxin between
194 6-12 hours. To test whether early depletion caused a developmental arrest, we used an
195 *hlh-8p::GFP* promoter reporter to monitor the M lineage (Harfe et al., 1998). Newly
196 hatched L1 animals have one M cell which undergoes a stereotypical series of divisions
197 to produce 16 M lineage cells by the L1 molt (Fig. S4A)(Sulston and Horvitz, 1977). We
198 shifted synchronized *nhr-23::AID*; *TIR1* animals carrying an *hlh-8p::GFP* reporter onto
199 auxin plates at 3 hours and 9 hours post-release. We imaged animals 24 hours post-
200 release and M cell number was scored (Fig S4B,C). *nhr-23::AID*; *TIR1* animals exposed
201 to auxin 3 hours post-release had an average count of 13.45 M cells while the late
202 exposure resulted in an average of 15.55 M cells (Fig. S4B). The *nhr-23::AID*; *TIR1*
203 animals exposed to auxin 9 hours post release did not have significantly different M cell
204 number than any of the controls ($p>0.3$)(Fig. S4C). These data suggest that *nhr-23::AID*;
205 *TIR1* animals exposed to auxin 3 hours post release were late L1 larvae. There are well-
206 characterized developmental checkpoints that promote larval arrest in the absence of
207 food (Fielenbach and Antebi, 2008; Kaplan and Baugh, 2016). *daf-16* is a transcription
208 factor which is part of the insulin signaling pathway and is necessary for starvation-
209 induced L1, L3, and L4 arrest (Baugh and Sternberg, 2006; Schindler et al., 2014).
210 Starved *daf-16* mutants fail to arrest at these checkpoints and continue development
211 (Baugh and Sternberg, 2006; Schindler et al., 2014). d*af-16* mutation did not significantly
212 alter M cell number when NHR-23 was depleted, suggesting the NHR-23-depletion
213 phenotype is independent from the insulin-signaling pathway (Fig. S4D).

214

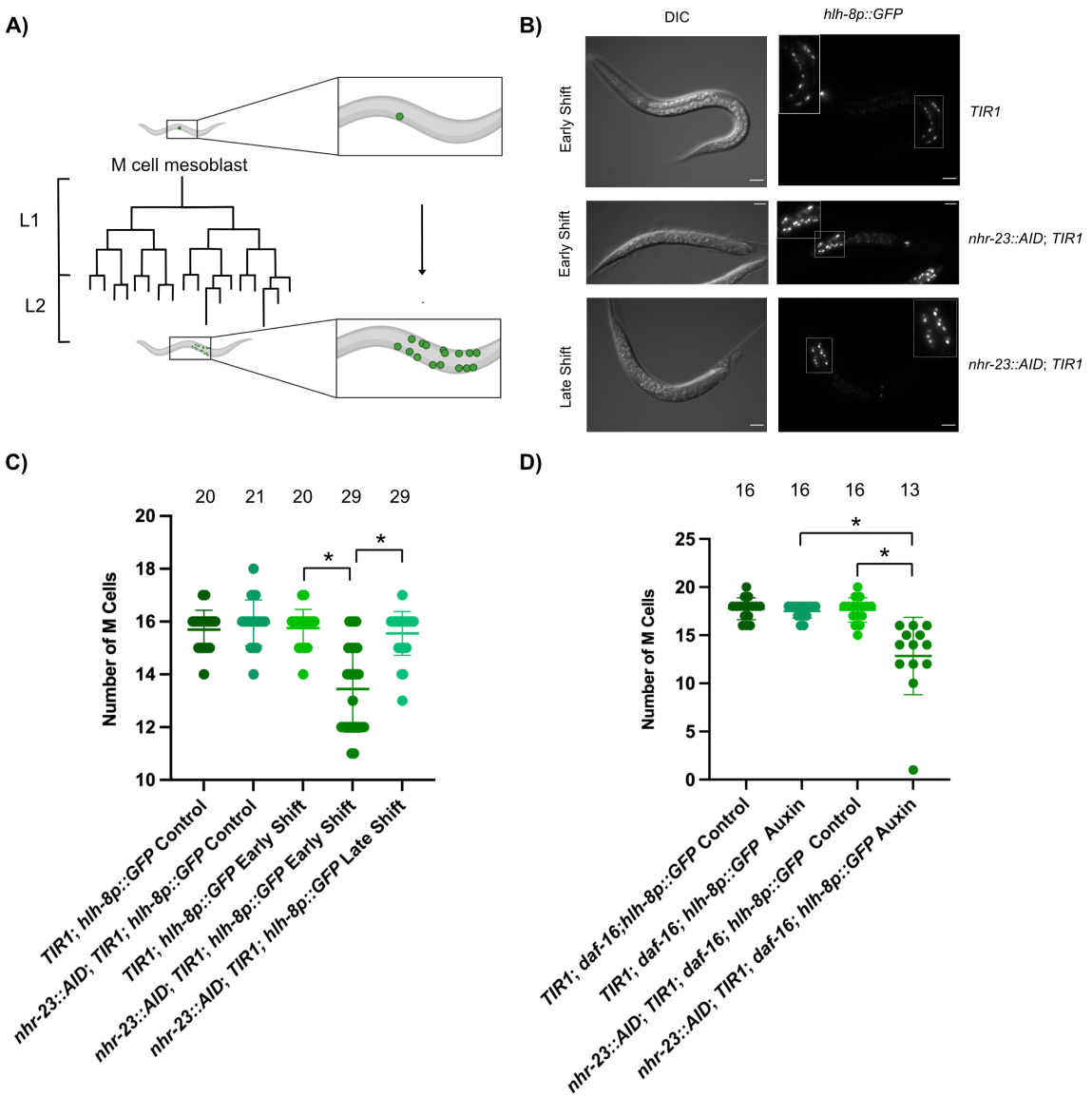

Fig. S4. NHR-23 depletion causes developmental delay which is *daf-16*-independent. (A) Depiction of the M cell mesoblast cell divisions in L1 larvae created with BioRender.com. Newly hatched animals are born with a single M cell, which undergoes the indicated set of divisions to produce 16 descendents at the L1/L2 molt. An *hlh-8p::GFP* reporter can be used to monitor M cell divisions in living animals. (B and C) Animals of the indicated genotype were synchronized and shifted to either auxin or control plates at either 3 (early shift) or 9 hours (late shift) post-release and imaged at 24 hours post-release. Two biological replicates were performed and animals examined are provided in (C). (B) Representative images of animals of the indicated genotypes on auxin plates. (C) M cell quantification for animals of the indicated genotype shifted to control or auxin plates. Mean and standard deviation are labeled. The number of animals assayed for each genotype and condition is indicated at the top of the graph (* two-tailed T-test p<0.0001). (D) M cell quantitation for synchronized animals of the indicated genotype shifted to auxin plates at 3 hours post-release and imaged 21 hours later (24 hours post-release). Mean and standard deviation labeled. The number of animals assayed for each genotype and condition is indicated at the top of the graph (* two-tailed T-test p<0.0001).

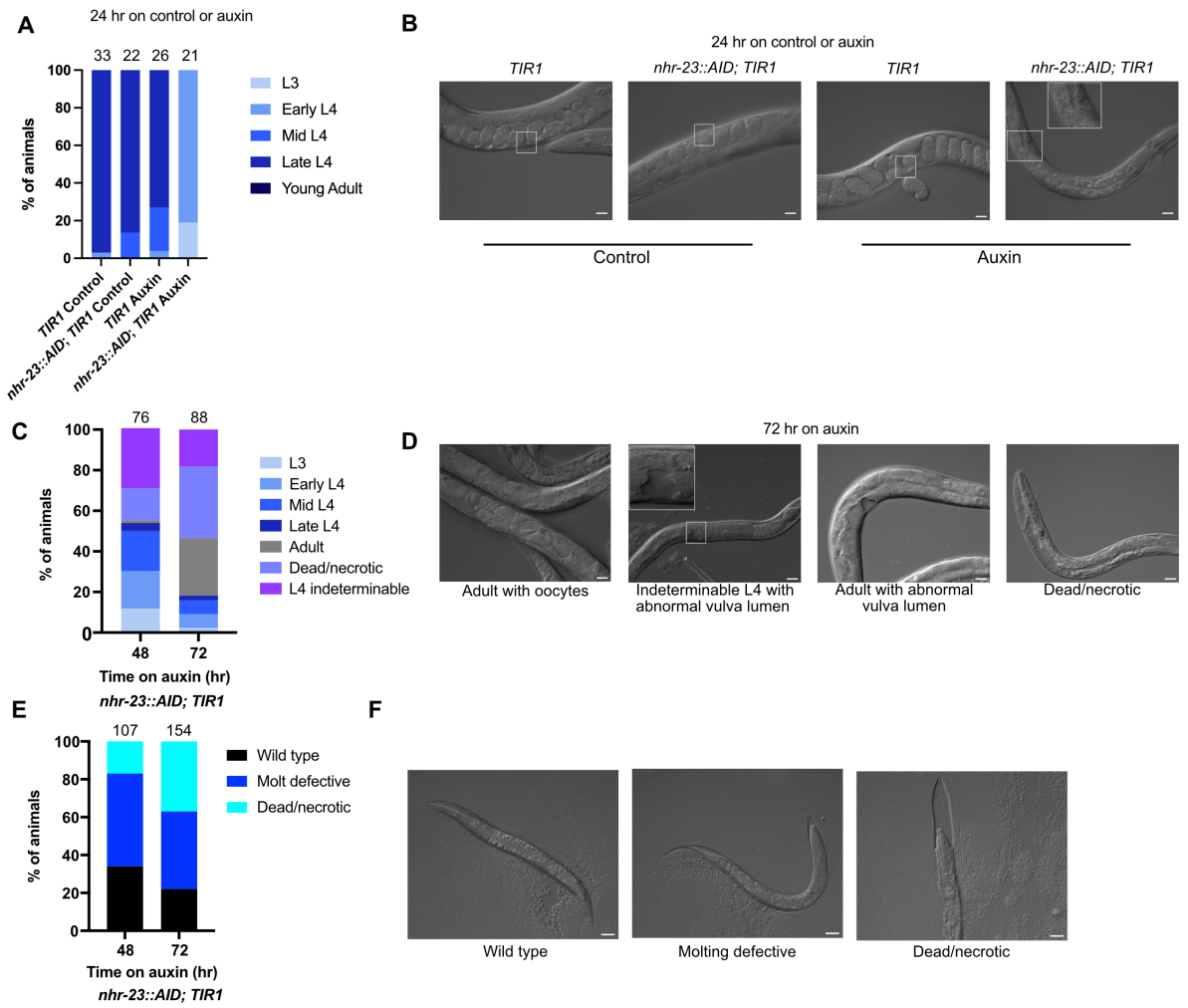

Fig. 3. NHR-23 depletion causes developmental delay. (A) Animals of the indicated genotype were synchronized and shifted onto auxin at 25 hours post-release and imaged 23 hours later (48 hours post-release). Animals were staged based on vulval morphology (Mok et al., 2015). L4 larval stages were grouped as Early L4 (4.0-4.2), Mid L4 (4.3-4.5), and Late L4 (4.6-4.9). (B) Representative images. The position of the vulva is highlighted with a white box. (C) *nhr-23::AID; TIR1* animals were treated as in (A) and staged after 48 and 72 hours on auxin. (D) Representative images. (E) Synchronized *nhr-23::AID; TIR1* L1 larvae were released on auxin and scored for molting defects and death 48 and 72 hours post-release. (F) Representative images. Images are representative of 100 animals examined over the course of two experiments. The number of animals assayed for each genotype and condition is indicated at the top of the graph in A, C, and E. Scale bars=20 µm. A zoomed inset is provided for the auxin-treated *nhr-23::AID, TIR1* images in B and D to highlight vulval morphology.

To distinguish between larval arrest and developmental delay, we performed depletion experiments later in development where we could use vulval morphology to score progression through the L4 stage. We performed depletion experiments shifting early L3 animals onto auxin and monitored development by scoring vulva morphology 24 hours later. The majority of TIR1 animals developed to late L4, with auxin causing a slight

220 developmental delay evidenced by more animals in mid-L4 (Fig. 3A,B). *nhr-23::AID*; *TIR1*
221 animals grown on control plates also reached late L4 displaying the same slight
222 developmental delay with a fraction of the population in mid-L4 (Fig. 3A,B). In contrast,
223 when *nhr-23::AID*; *TIR1* animals were shifted to auxin, the vast majority of animals were
224 early L4 larvae with a fraction of the population remaining in L3 (Fig. 3A,B). We repeated
225 these experiments, scoring *nhr-23::AID*; *TIR1* animals after 48 and 72 hours on auxin.
226 After 48 hours a fraction of the population had reached mid-L4 and after 72 hours we
227 observed adult animals as evidenced by the presence of oocytes (Fig. 3C,D). At both
228 timepoints there was a subset of L4 larvae which we could not precisely stage due to
229 aberrant vulval morphology (Fig. 3C,D); these animals had large vulval lumens
230 reminiscent of a 4.3 stage vulva (Mok et al., 2015), but we also observed adults with a
231 similar large vulval lumen (Fig. 3D). As animals progressed from 48 to 72 hours on auxin
232 we saw an increasing fraction of dead animals which appeared necrotic with large fluid
233 filled spaces within the animal (Fig. 3C,D). We then revisited our L1 depletion
234 experiments, plating synchronized L1 larvae directly onto auxin plates and scoring
235 animals 48 and 72 hours later. After 48 hours we observed animals with molting defects
236 and necrosis, the fraction of which increased after 72 hours on auxin (Fig. 3E,F).
237 Together, these data suggest that NHR-23 depletion causes developmental delay and
238 animals die due to a failed molt.
239
240 **NHR-23 regulates oscillating genes involved in aECM biogenesis and regulation of**
241 **protease activity**
242 To gain insight into how depletion of NHR-23 causes developmental delay, we analyzed
243 the expression of NHR-23-regulated genes by mining existing microarray (Kouns et al.,
244 2011) and oscillatory gene expression data (Hendriks et al., 2014)(Table S2). Of the 265
245 NHR-23 regulated genes, 236 (89%) were oscillatory (Table S2); a similar trend was
246 observed in a recent analysis of these datasets (Tsiairis and Großhans, 2021). In
247 contrast, 10-20% of *C. elegans* genes oscillate in expression (Hendriks et al., 2014; Kim
248 et al., 2013; Meeuse et al., 2020)(Two-tailed Chi-squared test $p<0.0001$). To test whether
249 these *nhr-23*-regulated oscillating genes were enriched for particular biological functions,
250 we performed gene ontology analysis which indicated an enrichment in genes implicated

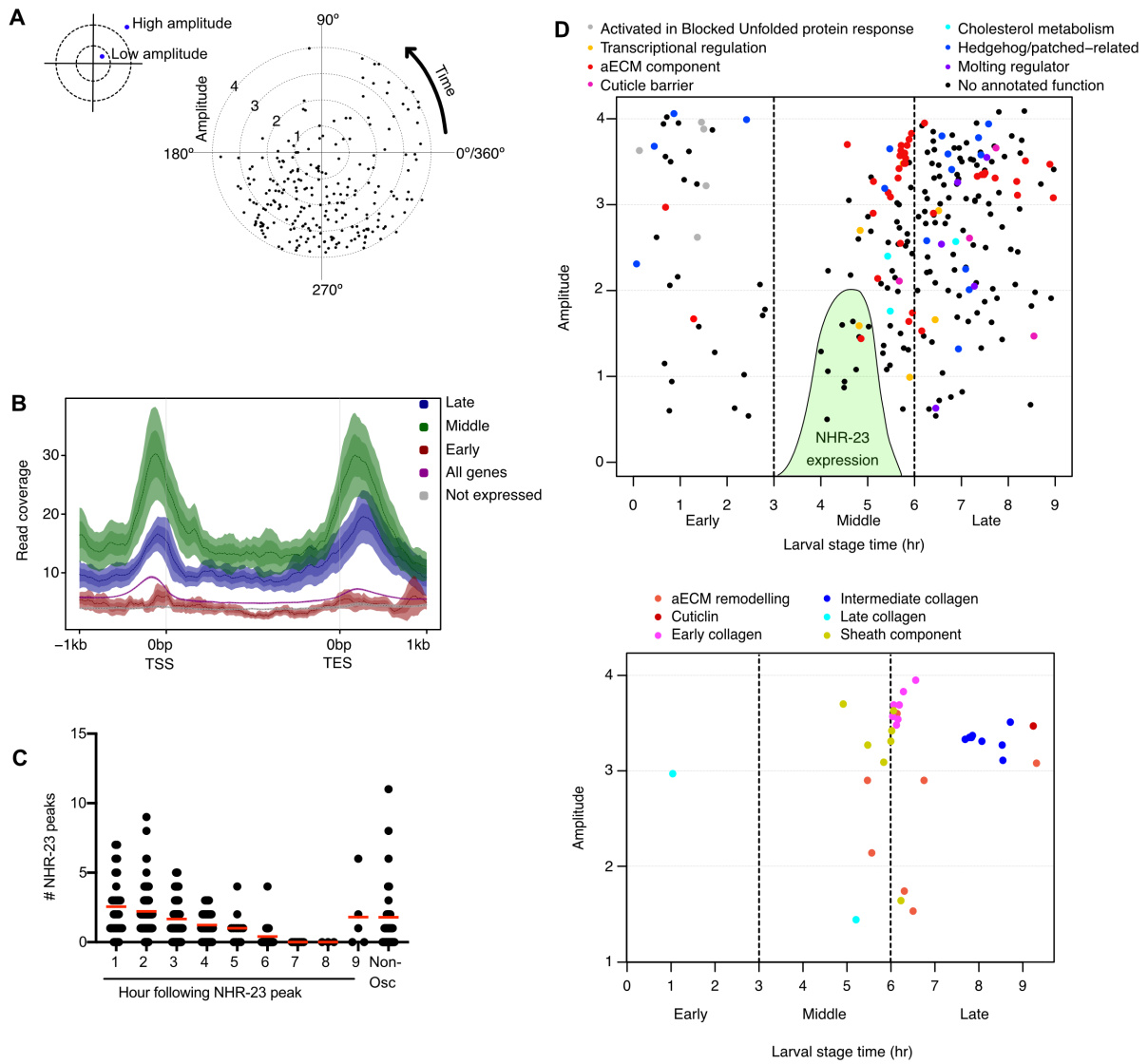

Fig. 4. NHR-23 regulates oscillating genes involved in aECM biogenesis. (A) Radar chart plotting amplitude over the phase of peak expression of *nhr-23*-regulated genes from Kouns *et al.* (2011). The dotted circles indicated amplitude, with the innermost circle representing an amplitude of 1 and the outermost circle representing an amplitude of 4. (B) Average signal from NHR-23 ChIP-seq data (Gerstein et al., 2010) for *nhr-23*-regulated oscillating genes with peak phases between 0º-120º (Early), 120-240º (Middle), and 240º-360º. *nhr-23* mRNA peaks at 178.11º. Signal is plotted relative to transcription start site (TSS) and transcription end site (TES). The average NHR-23 signal for all 21,600 *C. elegans* genes (All genes) and the 20% of genes with the lowest expression (No expression) are shown for reference. The mean signal is plotted with a line and the mean's 95% confidence interval is indicated by the shaded area. (C) Number of NHR-23 peaks flanking and within *nhr-23*-regulated genes. The genes are binned by their peak phase relative to the *nhr-23* peak phase. Non-oscillating (Non-Osc) *nhr-23* genes are also depicted. (D) The data from (A) was plotted as a scatter plot and functionally annotated (Table S2). We converted the 360º oscillation to developmental timing over a 9 hour larval stage so that 1 hour=40º. The green shaded area represents NHR-23 expression based on RNA-seq (peak phase=178.11º, amplitude=2.11; Meeuse et al., 2020), imaging (Figure 1B), and western blotting data (Figure 1C). Dotted lines in D and E indicate boundaries between the early, middle, and late *nhr-23*-regulated oscillating genes from B. (E) The genes in the aECM component class were subdivided into more specific classes and plotted as in D.

251

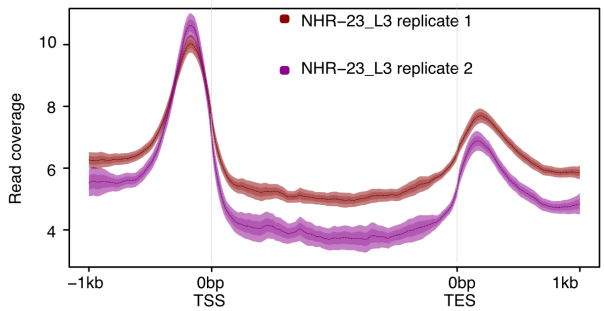

Fig. S5. NHR-23 enrichment around genes. Average signal over all aligned genes from two NHR-23 ChIP-seq replicates (Gerstein et al., 2010). The y-axis indicates non-normalized read coverage. The mean signal is plotted with a line and the mean's 95% confidence interval is indicated by the shaded area. TSS=transcription start site; TES=transcription end site.

in cuticle structure and regulation of endopeptidases (Table S3). These gene ontology classes are a specific subset of the functions enriched in all oscillating genes (Table S4). While the *C. elegans* genome encodes 181 collagen genes (Teuscher et al., 2019), *nhr-23* only regulated 13 collagens including all of the furrow collagens implicated in epidermal damage sensing and are in the "early" collagen group (Table S2 Fig. 4D,E); *dpy-2, dpy-3, dpy-7, dpy-10*)(Johnstone and Barry, 1996; Page and Johnstone, 2007; Dodd et al., 2018). Other *nhr-23*-regulated intermediate collagens have well-described roles in body morphology (*sqt-1, sqt-2, rol-6*; Fig. 4E)(Kramer and Johnson, 1993; Johnstone and Barry, 1996; Page and Johnstone, 2007). There are also several sets of genes involved in apical extracellular matrix biogenesis and remodeling, such as lipocalins, proteases, protease inhibitors, fibrillin, PAN and ZP domain-containing proteins, and leucine-rich repeat proteins (Fig. 4E). Although not enriched as a gene ontology class, NHR-23 also regulates several transcription factors implicated in molting or energy metabolism (*peb-1, nhr-91, dpy-20*)(Clark et al., 1995, 20; Fernandez et al., 2004; Kasuga et al., 2013). Most of the genes in these ontology classes have a peak phase following that of *nhr-23* (Fig. 4A,D,E).

To explore NHR-23 direct targets, we analyzed an NHR-23 L3 ChIP-seq dataset (Gerstein et al., 2010). As expected, NHR-23 was enriched in the promoter region of genes (Fig. 4B,S5, Table S5). There was also notable enrichment downstream of the transcriptional end site (Fig. 4B,S5, Table S5). We then examined whether NHR-23 was enriched near *nhr-23*-regulated oscillating genes (Table S2). We converted the period to developmental time assuming a 9 hour larval stage which makes each hour equivalent to 40º. We separated the genes into three groups based on their peak phase. There were

283 low levels of NHR-23 binding in genes that peaked in expression between 0 and 3 hours
284 (Fig. 4B); *nhr-23* mRNA peaks at 178.11º/4.45 hours (Meeuse et al., 2020). In contrast,
285 the genes that peaked in expression between 3 and 6 hours had much higher NHR-23
286 binding (Fig. 4B). The genes peaking in expression later (6-9 hours) had reduced NHR-
287 23 binding, but still higher levels than the genes peaking between 0 and 3 hours (Fig. 4B).
288 Genes which peak in expression close to when *nhr-23* mRNA levels peak tend to have
289 higher NHR-23 levels upstream, downstream, and within their gene bodies (Fig. 4B).
290 Consistent with these data, there tended to be more NHR-23 peaks flanking and within

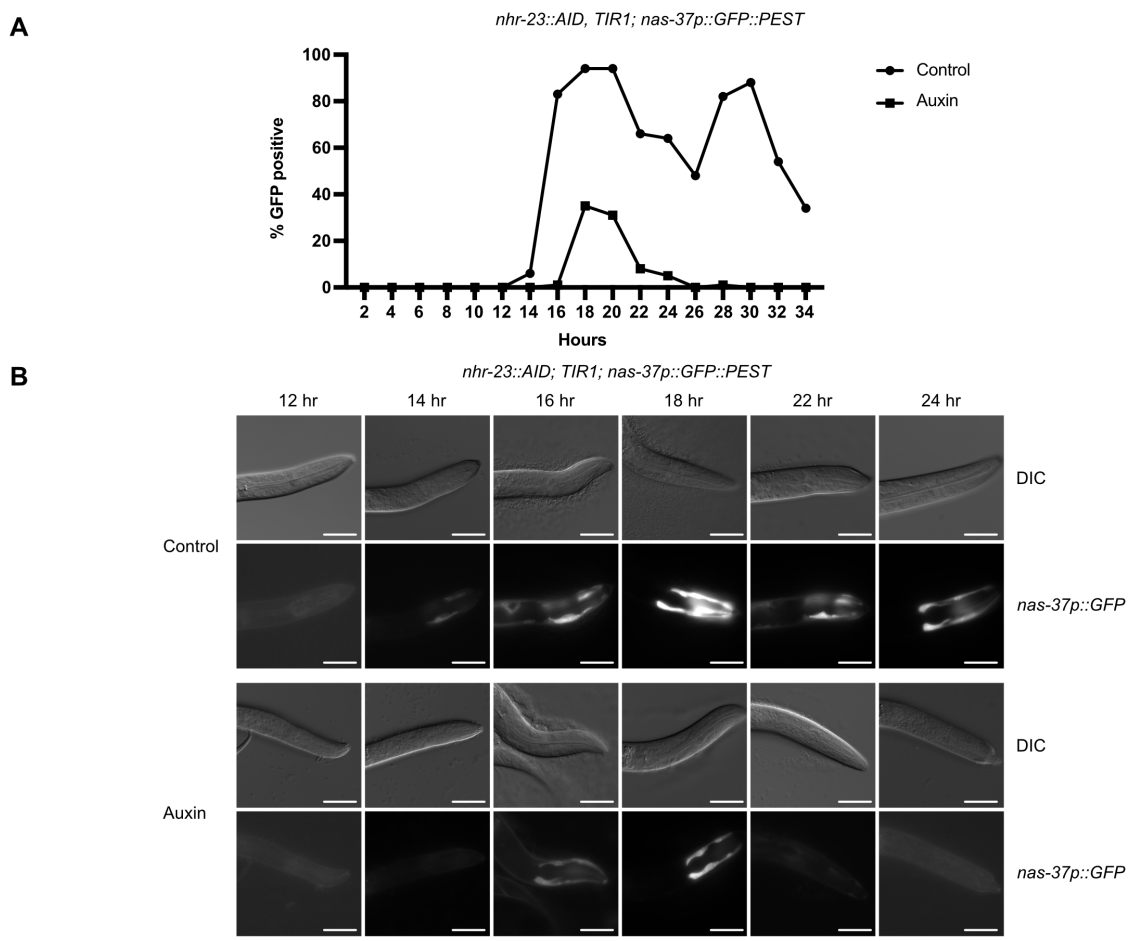

Fig. 5. NHR-23-depletion causes reduced expression of an *nas-37p::GFP::PEST* promoter reporter. (A) *nas-37p::GFP::PEST* expression time course. *nhr-23::AID, TIR1; nas-37p::GFP::PEST* animals were synchronized and released on control or auxin plates and scored for head or hypodermal GFP expression every two hours. Fifty animals per time point were scored in two independent experiments and the percentage of animals expressing GFP are presented. (B) Representative images of *nhr-23::AID, TIR1, nas-37p::GFP::PEST* animals grown on control or auxin plates at the indicated time points. Scale bars=20 µm.

291 *nhr-23*-regulated genes that had peak expression close to the *nhr-23* peak expression (1-
292 4 hours) compared to those that peaked later (5-8 hours) (Fig. 4C).
293
294 As NHR-23-regulated oscillating genes were enriched in proteases and protease
295 regulators (Table S2), we tested how NHR-23 depletion affected expression of a *nas-37*
296 promoter reporter; *nas-37* is a protease implicated in *C. elegans* ecdysis (Davis et al.,
297 2004). We released synchronized *nhr-23::AID, TIR1* animals carrying a *nas-*
298 *37p::GFP::PEST* reporter onto control and auxin plates and monitored GFP expression
299 over development. Animals growing on control media displayed oscillating reporter
300 activity with peaks at 18 and 30 hours (Fig. 5A,B). NHR-23 depleted animals exhibited a
301 delayed onset of reporter expression and only a subset of animals expressed the reporter
302 (Fig. 5A,B). There was only one pulse of *nas-37p::GFP::PEST* expression after which we
303 detected no reporter activity (Fig. 5A,B). Together, these data confirm that NHR-23
304 regulates *nas-37* expression and that following NHR-23-depletion there is a weaker pulse
305 of target gene expression followed by a failure to express again.
306
307 **NHR-23-depletion causes defects in aECM structure and function**
308 Defects in cuticle collagen patterns have been observed in *nas-37* mutants (Davis et al.,
309 2004), so we examined whether NHR-23 depletion affected aECM structure. We used
310 CRISPR/Cas9-mediated genome editing in *nhr-23::AID; TIR1* animals to introduce
311 mNeonGreen (mNG)::3xFLAG cassettes into three genes in: i) *rol-6*; an intermediate
312 collagen ii) *bli-1,* a collagen that forms struts in the adult cuticle; and iii) *noah-1*, a
313 component of the transient sheath. *rol-6* and *noah-1* were regulated by *nhr-23* while *bli-1*
314 is an adult-specific collagen expressed in L4 larvae, so would not be interrogated in the
315 microarray experiment (Kouns et al., 2011). We first confirmed that each knock-in had a
316 wild-type brood size (Fig S6A) and then tested fusion protein size by western blotting.
317 Anti-FLAG immunoblotting on *nhr-23::AID; TIR1, rol-6::mNG::3xFLAG* lysates detected a
318 single band of the expected size (~70 kDA; Fig S6B). In *noah-1::mNG::3xFLAG, nhr-*
319 *23::AID; TIR1* lysates there was a band of the expected size (~150 kDa) as well as a
320 lower ~50 kDa band. *noah-1* is only predicted to have a single isoform so this might reflect
321 a cleavage or degradation product. In *nhr-23::AID; TIR1, bli-1::mNG::3xFLAG* there were

A

Genotype	Brood size (±std. dev.)
Wild type	290±48
nhr-23::AID; TIR1, rol-6::mNG	293±48
nhr-23::AID; TIR1, bli-1::mNG	236±56
noah-1::mNG, nhr-23::AID; TIR1	246±27

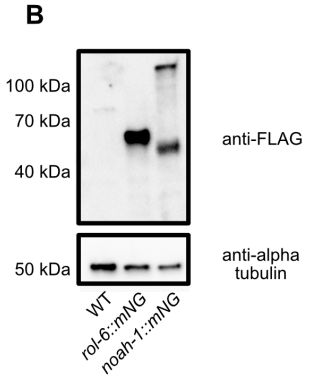

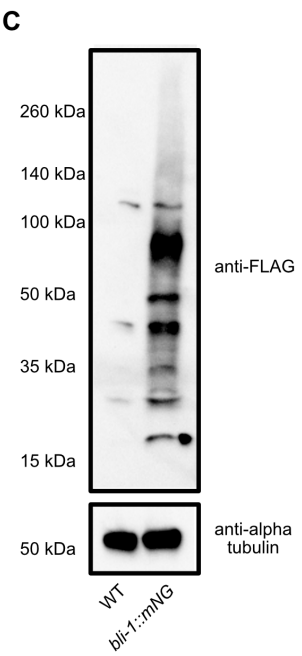

Fig. S6. Validation of *bli-1, noah-1,* and *rol-6* mNeonGreen::3xFLAG knock-in strains. (A) Brood size analysis of animals of the indicated genotype. Anti-FLAG immunoblots on lysates from *rol-6::mNG* and *noah-1::mNG* mid-L4 animals (B) and *bli-1::mNG* adult animals (C). An age matched WT control is included in each experiment. Marker size (in kDa) is provided and an anti-alpha-tubulin immunoblot was used as a loading control. The mNeonGreen::3xFLAG tag adds ~33.2 kDa and the predicted sizes are: ROL-6::mNG=67.9 kDa; NOAH-1::mNG=148.9 kDA; BLI-1::mNG=138.5 kDa.

322 several prominent bands smaller than the ~140 kDa predicted product (Fig S6C). These
323 might reflect processing, which is common with collagens (Myllyharju and Kivirikko,
324 2004).
325
326 ROL-6 is a component of the L2, L3, L4 and adult cuticle. Expression in L1 larvae is first
327 observed 14-16 hours post-release and subsequently is incorporated into annuli in the
328 aECM (Fig. 6A). When we depleted NHR-23 in L3 larvae ROL-6::mNG expression
329 appeared unaffected, but the annular localization was irregular and thicker and we
330 observed gaps in the annular ROL-6::mNG over the seam cells (Fig. 6B). Many animals
331 had a corset of unshed cuticle to which ROL-6::mNG localized (Fig. 6C). We next
332 addressed whether NHR-23 depletion affected the formation of struts in the cuticle medial
333 layer. BLI-1 expression is first detected in hypodermal cells in stage 4.5 L4 larvae (Fig.
334 6D) where it also decorates annuli (Fig. 6E). It then becomes incorporated into struts by
335 late L4 (Fig. 6F). We shifted *nhr-23::AID; TIR1, bli-1::mNG* animals onto control or auxin

336

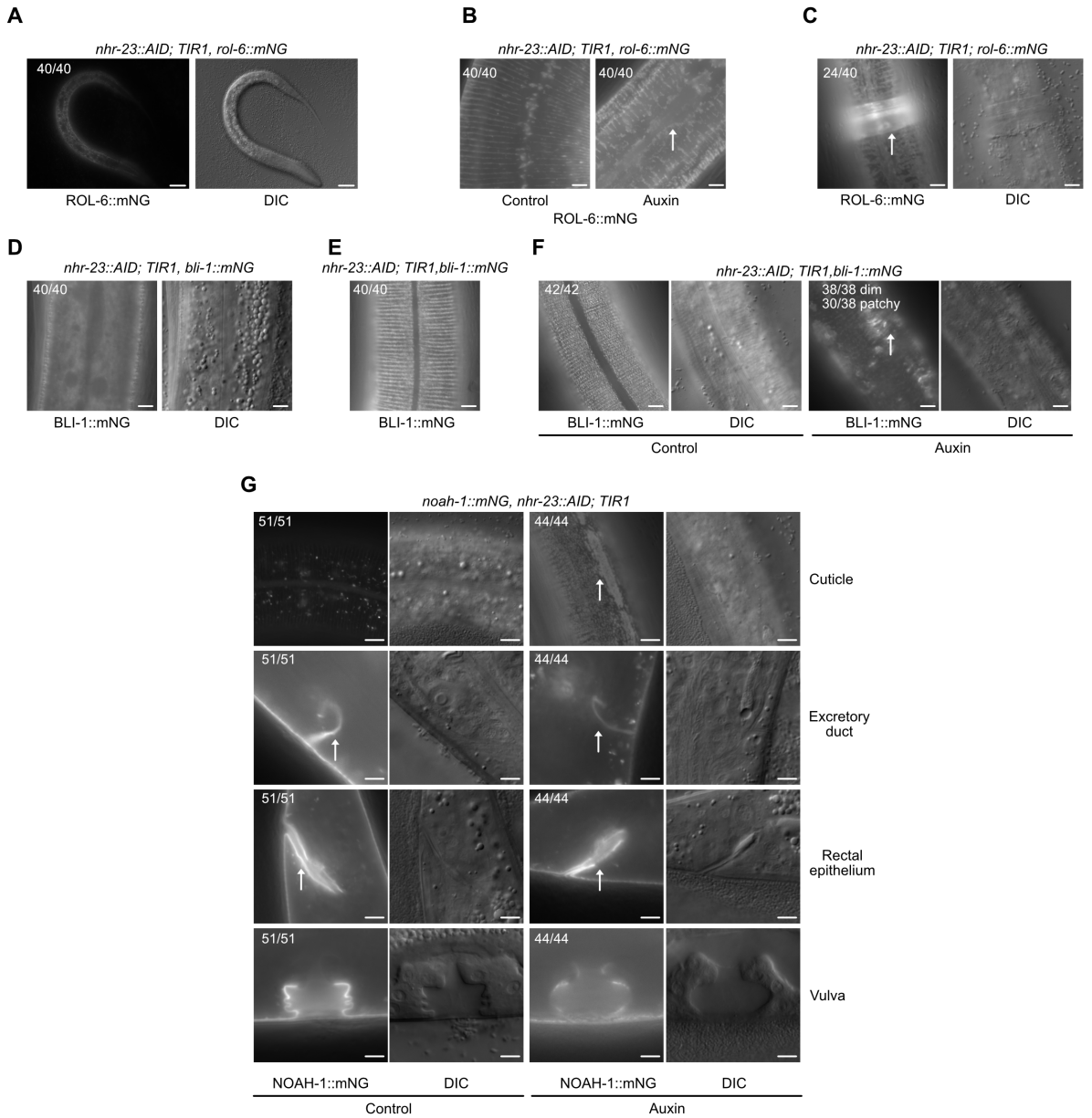

Fig. 6. NHR-23-depletion causes ROL-6 and NOAH-1 localization defect and reduced expression and mislocalization of BLI-1. (A) ROL-6::mNG is first observed internally in epidermal cells 14-16 hours post-release. (B) Representative GFP images of *nhr-23::AID; TIR1, rol-6::mNeonGreen::3xFLAG* (*rol-6::mNG*) animals grown on control or auxin plates. Arrow indicates gap over seam cells (C) Representative images of *nhr-23::AID; TIR1, rol-6::mNG* animals grown on auxin with a corset phenotype. Corset is indicated by arrow. ROL-6::mNG is first observed internally in epidermal cells 14-16 hours post-release. BLI-1::mNG is first observed internally in L4.5 animals (D) where it also localized to annuli (E). Representative GFP and DIC images of *nhr-23::AID; TIR1, bli-1::mNeonGreen::3xFLAG* (*bli-1::mNG*) animals grown on control or auxin plates. Patch of BLI-1::mNG indicated by arrow. (G) Representative GFP and DIC images of the indicated tissues of *noah-1::mNeonGreen::3xFLAG* (*noah-1::mNG*), *nhr-23::AID; TIR1,* animals grown on control or auxin plates. NOAH-1::mNG gap over seam cells, and localization to excretory duct and rectum are indicated by arrows. The number of animals examined and for which the images are representative from two biological replicates is shown in A-G. Scale bars=20 μm for all images except the *noah-1::mNG* excretory duct, rectal epithelium, and vulva (scale bar=5 μm for these images).

337 plates in early L3 and examined BLI-1::mNG expression and localization. We scored
338 control animals after 24 hours on auxin when animals were late L4s and needed to score
339 NHR-23 depleted animals 24 hours later due to the developmental delay. NHR-23
340 depletion caused reduced expression of BLI-1::mNG and a loss of the punctate pattern
341 (Fig. 6F). BLI-1::mNG weakly localized to annuli and animals displayed bright,
342 disorganized patches of BLI-1::mNG (Fig. 6F).
343
344 Based on the defects in ROL-6 and BLI-1 localization, we next examined whether NHR-
345 23 depletion affected formation of the sheath, a transient pre-cuticular structure thought
346 to play a role in patterning the cuticle (Cohen and Sundaram, 2020). NOAH-1 is a zona
347 pellucida domain protein that is part of the pre-cuticular aECM in embryos and larvae. In
348 L4 larvae, we observed the reported vulval lumenal localization and cuticular expression
349 (Cohen et al., 2020), as well as localization to the rectum and excretory duct (Fig. 6G).
350 NHR-23 depletion did not affect NOAH-1 localization in the excretory duct or rectum.
351 Although vulval morphology is aberrant in NHR-23-depleted animals, NOAH-1 still
352 localizes to cell surfaces (Fig. 6G). In mid-L4, NOAH-1 is normally localized to the cuticle
353 and lysosomes and is absent from over the seam cells (Fig. 6G). NHR-23-depletion
354 caused a loss of NOAH-1::mNG localization to annulli (Fig. 6G). Instead, we observed
355 small irregular punctae and accumulation of NOAH-1::mNG over seam cells (Fig. 6G).
356 Together, these data indicate that NHR-23 depletion leads to defective localization of
357 proteins in both the collagenous cuticle and the sheath.
358
359 Given the defects in aECM structure following NHR-23-depletion, we tested whether the
360 epidermal barrier was intact. First, we incubated control and auxin-treated *nhr-23::AID,*
361 *TIR1* animals with the cuticle impermeable, cell membrane permeable Hoechst 33258
362 dye which stains nuclei. N2 and *TIR1* animals grown on control or auxin plates exhibited
363 low Hoechst staining in the head (4-15%) and body (0-0.7%). *nhr-23::AID, TIR1* animals
364 grown on control plates exhibited higher head staining (40%) but no body staining, while
365 almost all animals on auxin plates displayed Hoechst staining in their head and body (96%
366 and 99%, respectively) (Fig. 7A). Animals shifted onto auxin early or late in L1 robustly
367 expressed an *nlp-29p::GFP* reporter (Fig. 7B,C), which can be activated by infection,

368

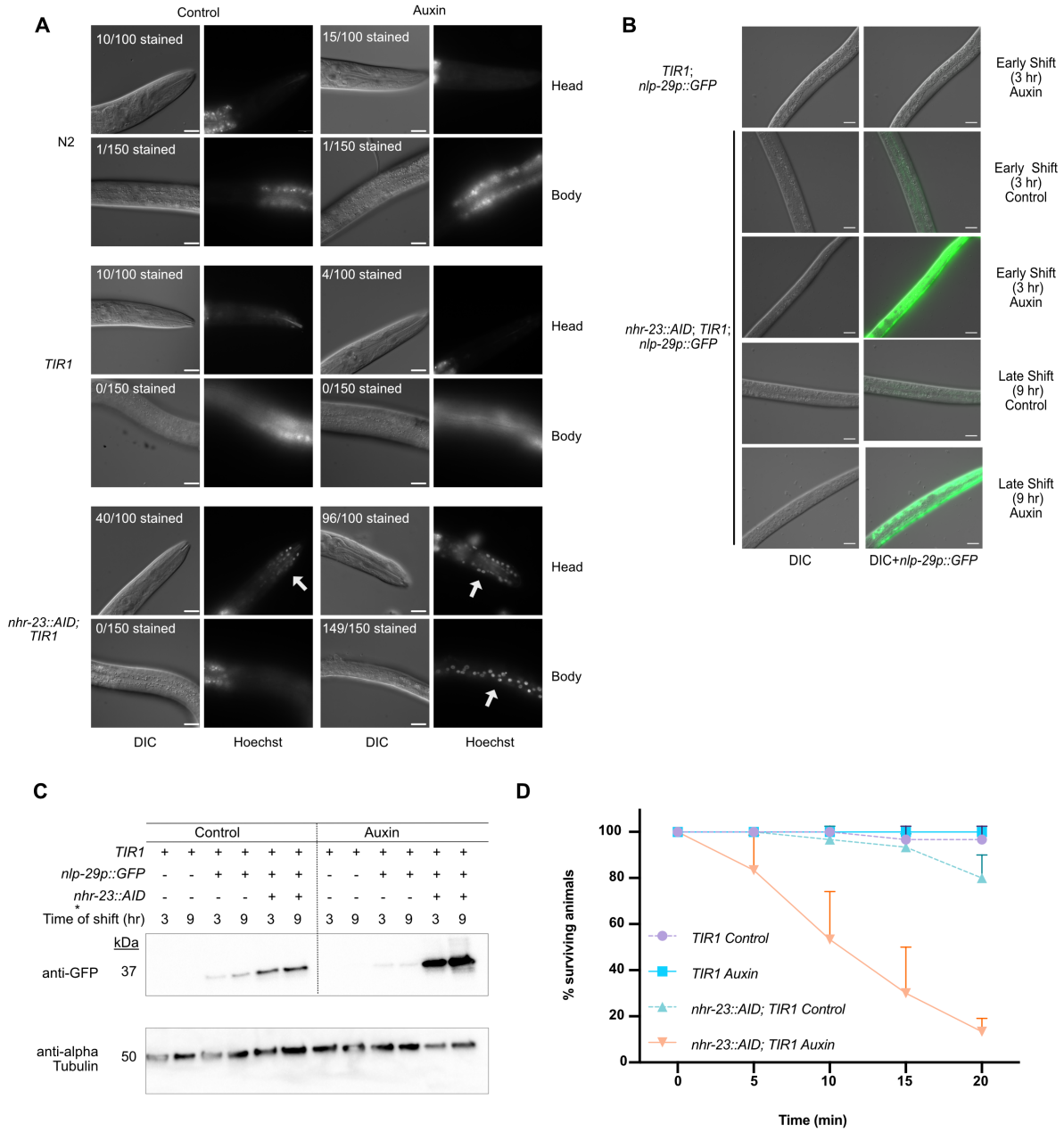

Fig. 7. Depletion of NHR-23 leads to a defective cuticle barrier (A) Permeability to Hoechst 33258 dye. Synchronized animals of the indicated genotype were shifted onto control or auxin plates at 25 hours post-release and grown for 24 hours. Animals were washed off plates and incubated with the cuticle impermeable/membrane permeable Hoechst 33258 dye and scored for nuclear staining in the head and body. The data are from two biological replicates. Scale bars=20µm. Non-nuclear fluorescence in the body is background. (B) Representative images of GFP expression in animals of the indicated genotype following an early and late shift to control or auxin plates. The images are representative of 50 animals observed during each of two experimental replicates. (C) Anti-GFP immunoblot analysis of *nlp-29::*GFP expression. Marker size (in kDa) is provided. Stain-free analysis, which visualizes total protein on the membrane, is provided as a loading control. The blots are representative of two experimental replicates. (D) *nhr-23::AID; TIR1* and *TIR1* animals were added to 20µl of dH_20 and viability was assessed every five minutes. Ten animals were assayed for each genotype and condition with three biological replicates.

369 acute stress, and physical damage to the cuticle (Pujol et al., 2008; Zugasti and Ewbank,
370 2009). We further tested the cuticle integrity in a hypo-osmotic shock assay in which
371 animals with defective cuticle barriers rapidly die following exposure to water (Kage-
372 Nakadai et al., 2010). *TIR1* animals grown on control media or auxin were completely
373 viable in water (Fig. 7D). *nhr-23::AID, TIR1* control animals had a weakly penetrant
374 sensitivity to hypo-osmotic shock, while the same strain grown on auxin rapidly died
375 following hypo-osmotic shock (Fig. 7D). These data suggest that NHR-23 is required for
376 the cuticle barrier.
377
378 ***nhr-23* is necessary in seam and hypodermal cells for larval development**
379 Finally, we wished to determine in which cells *nhr-23* was necessary for larval
380 development through a tissue-specific RNAi approach. In RNAi-proficient N2 animals,
381 100% of *nhr-23(RNAi)* animals exhibited developmental delay and molting defects (Fig.
382 8A-C). *nhr-23* knockdown in body-wall muscle and intestinal cells produced no molting
383 defects and we observed only mild developmental delay (0-11.5% of animals)(Fig. 8A-
384 C). Vulval precursor cell-specific *nhr-23(RNAi)* caused molting defects in 23.4% of
385 animals and we also observed developmental delay in 22.1% of animals. We observed
386 highly penetrant developmental delay (90.4%) and molting defects (39.9%) when we
387 performed *nhr-23* RNAi in a strain using a *wrt-2* promoter for tissue-specific RNAi (Fig.
388 8A-C). *wrt-2* is expressed in seam cells, rectal cells and hypodermal cells (Fig. S7C,D;
389 Aspöck et al., 1999). Given this result and the defective ROL-6::mNG and NOAH-1::mNG
390 (Fig. 6) localization over seam cells, we generated more tissue-restricted RNAi strains.
391 We used a minimal seam cell-specific enhancer with a *pes-10* minimal promoter (Ashley
392 et al., 2021), which is robustly expressed in seam cells with some weak hypodermal
393 expression (Fig. S7A,B). To test the specificity of this strain, we introduced a *his-72::mNG*
394 knock-in. In control animals, we observed nuclear expression in seam, hypodermal,
395 intestinal, vulval and germline cells, as expected for a histone H3 fusion (Fig S8).
396 *mNeonGreen* RNAi caused reduced HIS-72::mNG expression in seam, hypodermal
397 syncytium, and intestinal nuclei. *nhr-23(RNAi)* in the *SCMp* RNAi strain phenocopied *nhr-*
398 *23(RNAi*) in N2 animals with almost all animals exhibiting developmental delay (99.3%)
399 and molting defects (98.7%)(Fig. 8A-C). Notably, intestine-specific *nhr-23* RNAi did not

A

Strain	Promoter for tissue-specific RNAi	Tissue-specific RNAi	RNAi	N
N2	N/A	Whole animal	Control	362
			nhr-23	272
WM118	*myo-2p*	Body muscle	Control	252
			nhr-23	320
VP303	*nhx-2p*	Intestine	Control	317
			nhr-23	393
MGH171	*vha-6p*	Intestine	Control	602
			nhr-23	573
JU2039	*lin-31p*	Vulval precursor cells	Control	325
			nhr-23	367
QK52	*wrt-2p*	Seam cell, hypodermis, rectum	Control	299
			nhr-23	198
JDW371	*SCMp*	Seam cell, some hypodermal	Control	232
			nhr-23	153
JDW510	*suro-1p*	Hypodermis	Control	259
			nhr-23	211

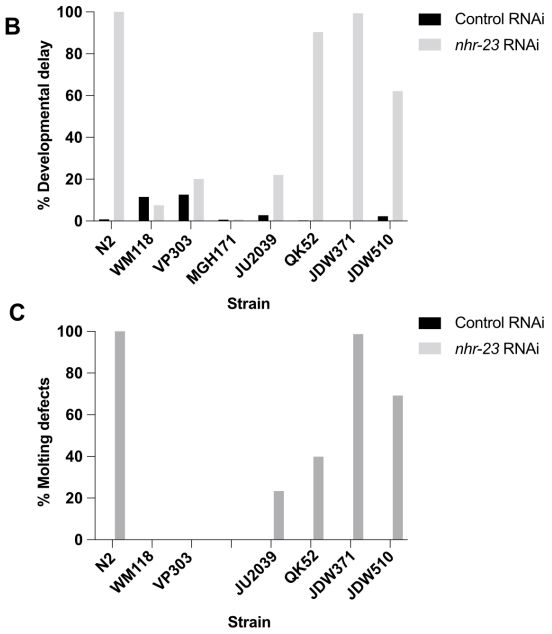

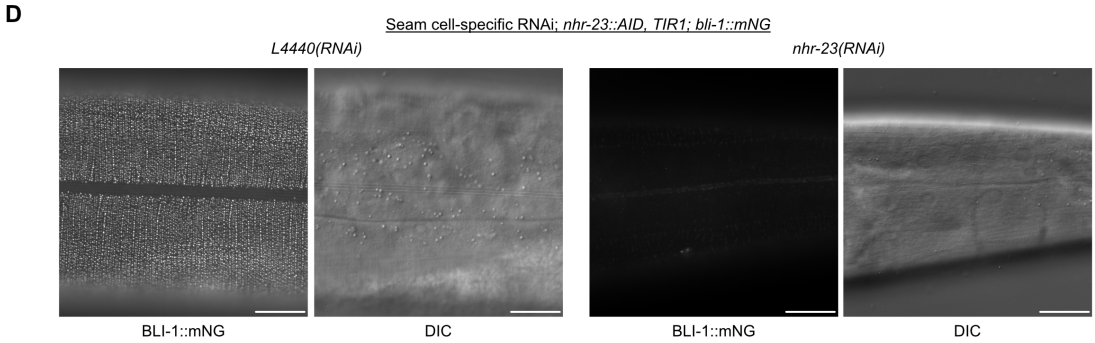

Fig. 8. *nhr-23* is necessary in seam cells for developmental progression, molting and BLI-1 localization. (A) Tissue-specific RNAi strains used. A timed egg lay of animals of the indicated genotype were performed on control or *nhr-23* RNAi plates and plates were scored three days later. The number of progeny scored from two biological replicates is indicated. (B) Developmental delay was scored in the indicated strains and classified as a failure to reach adulthood after 72 hours of growth. (C) Molting defects were scored in the indicated strains and included animals trapped in cuticles, animals dragging cuticles, and animals with cuticle corsets.

400 cause phenotypes (Fig. 8A-C). We then constructed a hypodermis-specific RNAi strain
401 using the *semo-1* promoter (Kaletsky et al., 2018; Köhnlein et al., 2020). *nhr-23* RNAi in
402 this strain produced molting defects and developmental delay, though with less
403 penetrance compared to our *SCMp*-specific RNAi strain (Fig 8A-C). To test the effect of
404 *SCMp*-specific *nhr-23* knockdown on the aECM, we introduced a BLI-1::mNG knock-ins
405 in our seam cell-specific RNAi strain. *nhr-23* depletion in this strain caused reduced BLI-
406 1 levels, similar to NHR-23 protein depletion in the soma (Figs. 6F, 8D). BLI-1::mNG also
407 was observed over the seam cells, which does not occur in wild-type animals (Fig. 8D).

408 Together these data indicated that *nhr-23* is necessary in the seam and hypodermal cells
409 for timely developmental progression, completion of molting, and aECM formation.
410

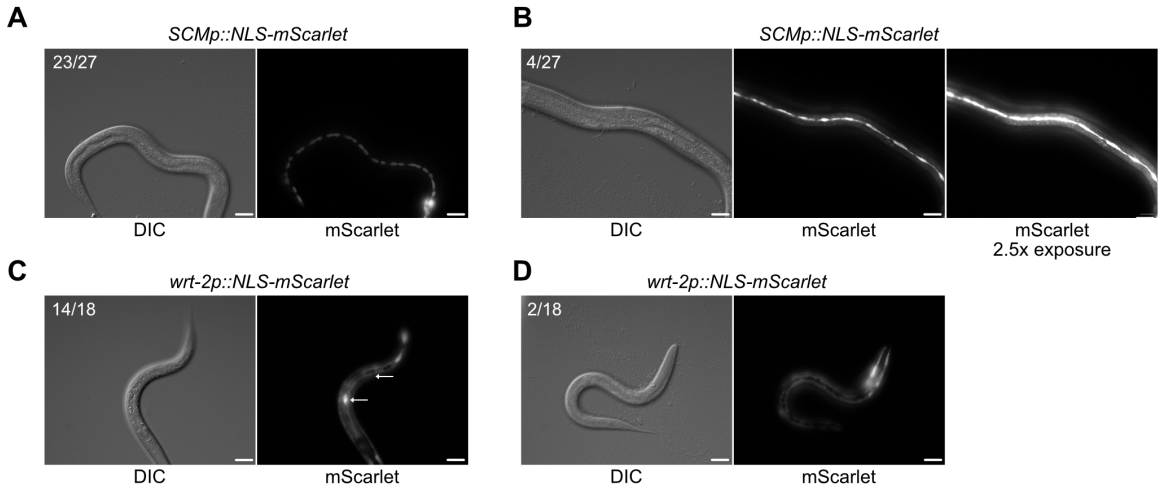

Fig. S7. Expression patterns of *SCMp* and *wrt-2* promoter reporters. *SCMp::NLS::mScarlet* promoter reporters express robustly in the seam cells (A) with weak expression in the hypodermis (B) in a subset of animals. *wrt-2p::NLS::mScarlet* is expressed in the hypodermis and seam cells (C and D). In some animals seam cell expression is lacking. In C, arrows point to two seam cells, one with reporter expression and one lacking it. Two biological replicates were performed and the number of animals for which each image is representative is indicated.

411 **DISCUSSION**

412 *C. elegans* molting is a powerful system to understand developmentally programmed
413 aECM regeneration. In this study**,** we determine when and where NHR-23 acts and how
414 it promotes aECM regeneration. NHR-23 oscillates and depletion early in L1 larvae
415 causes severe developmental delay. NHR-23-depletion in L3 larvae causes a similar
416 delay during the L4 stage. *nhr-23*-regulated genes are enriched for cuticle components
417 and protease inhibitors, and NHR-23 is enriched at the transcription start and end sites
418 of target genes. NHR-23-depletion causes aberrant localization of the early collagen
419 ROL-6 and the pre-cuticle component, NOAH-1. It also causes severely reduced levels
420 of the medial layer collagen BLI-1, which is also mislocalized. These cuticle defects are
421 correlated with a loss of the cuticle barrier. Tissue-specific RNAi suggested that *nhr-23* is
422 necessary in seam and hypodermal cells.
423
424

425

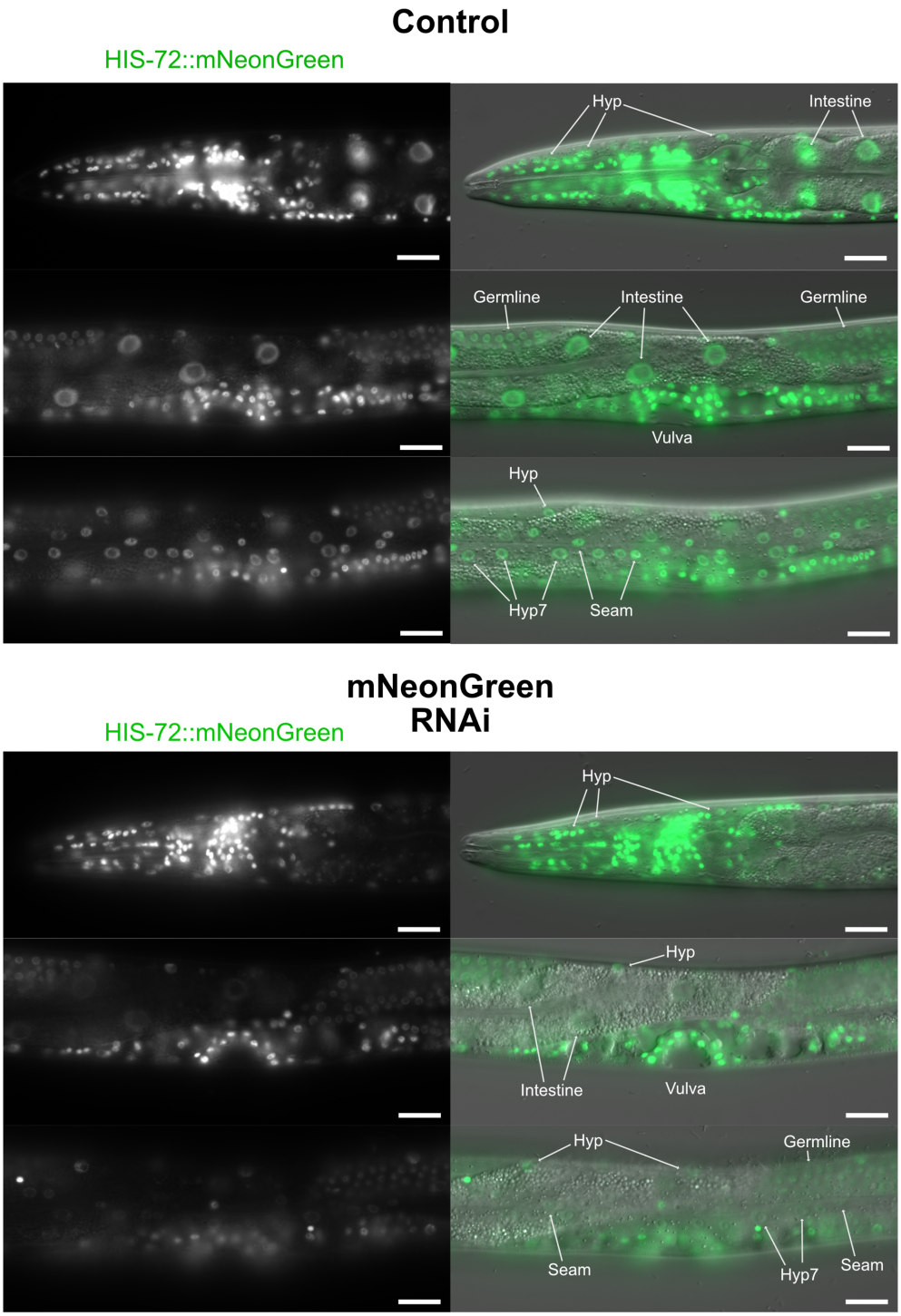

Fig. S8. JDW525 animals are permissive for RNAi knockdown in seam, hypodermal, and intestinal cells. JDW 525 [*his-72(wrd142[mNeonGreen::his-72]) III ; jsTi1493 {mosL loxP [wrdSi65(SCMp::rde-1 CDS+3'UTR)] FRT3::mosR} IV ; rde-1 (ne300) V]* animals grown on control RNAi display HIS-72::mNG expression in hypodermal, intestinal, germline, vulval, and seam cells. mNeonGreen RNAi caused reduction of HIS-72::mNG expression in seam, intestinal, and syncytial hypodermal (hyp7) cells. Vulval, germline, and head hypodermal expression was unaffected. Scale bars=20µm. Data are representative of forty animals examined over two biological replicates.

426 **NHR-23 is necessary for cuticle structure and function**

427 Integration of *nhr-23(RNAi)* microarray and NHR-23 ChIP-seq datasets suggests that
428 NHR-23 regulates a set of pre-cuticle, early collagen, protease inhibitor genes (Gerstein
429 et al., 2010; Kouns et al., 2011). NHR-23 binds more robustly in the promoter and
430 transcription end site of genes which peak in expression closer to the *nhr-23* mRNA peak
431 in expression (Fig. 4). One intriguing possibility is that the earlier NHR-23-regulated genes
432 may be more sensitive to NHR-23 levels. Consistent with this model, there appear to be
433 more NHR-23 peaks flanking and within early *nhr-23*-regulated genes (Fig. 4, Tables S2,
434 S5). This model would align with *E. coli* amino acid biosynthesis gene regulation where
435 enzymes earlier in the pathway have more responsive promoters with higher activity
436 (Zaslaver et al., 2004). We validated that NHR-23 regulates the expression of *nas-37*, a
437 protease implicated in molting (Fig. 5). Curiously, two other targets (*noah-1, rol-6*)
438 seemed to be expressed at near wild-type levels, but displayed aberrant localization (Fig.
439 6). These data highlight a potential limitation of a single time point gene expression study.
440 A shift in phase of an oscillating gene without change in amplitude could create the
441 appearance of up- or down-regulation depending on the sampling time point (Tsiairis and
442 Großhans, 2021). The *nhr-23(RNAi)* microarray is a useful starting point to understand
443 how NHR-23 promotes molting, but an RNA-seq time course on NHR-23 depleted
444 animals may be necessary to identify regulated genes. Such an approach was necessary
445 to determine how the pioneer factor, BLMP-1, promotes developmental timing (Hauser et
446 al., 2021).

447

448 NHR-23-depletion caused aberrant localization of NOAH-1 and ROL-6, lower levels of
449 BLI-1 (Fig. 6) and a severe barrier defect (Fig. 7). There are numerous *nhr-23*-regulated
450 genes which are implicated in the epithelial barrier. The cuticle furrow formed by six *nhr-*
451 *23*-regulated collagens (*dpy-2, dpy-3, dpy-7, dpy-8, dpy-9, dpy-10*) is thought to be
452 monitored by a sensor which coordinates a number of stress responses following
453 detection (Dodd et al., 2018). An RNAi screen of 91 collagens found that inactivation of
454 only these six collagens caused a barrier defect (Sandhu et al., 2021). Inactivation of a
455 subset of the furrow collagens causes permeability to Hoechst 33458 dye and elevated
456 *nlp-29p::GFP* reporter activity (Dodd et al., 2018), consistent with our NHR-23-depletion

457 data (Fig. 7). *bus-8* is a predicted glycosyltransferase that plays a role in the epithelial
458 barrier and is also *nhr-23*-regulated and its peak expression follows that of the furrow
459 collagens (Table S2). Screening *nhr-23* regulated genes may find other genes implicated
460 in the epithelial barrier and the peak phase could provide insight into how this barrier is
461 constructed.
462
463 **NHR-23 acts in seam and hypodermal cells to promote molting**
464 When we depleted NHR-23 early in L1, animals appeared wild type with few molting
465 defects, whereas later depletion produced strong molting defects (Fig. 2). This difference
466 in phenotypes reflected severe developmental delay when we depleted NHR-23 early in
467 L1. A similar result was observed when we depleted NHR-23 in L3 larvae; it took an extra
468 48 hours for animals to reach late L4 or early adulthood (Fig. 3). This observation is
469 consistent with RNAi data demonstrating that *nhr-23* knockdown causes developmental
470 delay, while overexpression accelerates development (Macneil et al., 2013; Meeuse et
471 al., 2022). An NHR-23-regulated promoter reporter (*nas-37p::GFP::PEST*) peaked at a
472 similar time in control and NHR-23-depleted animals (Fig. 5), but was expressed at lower
473 levels. This data might suggest that the low levels of NHR-23 present are sufficient to
474 drive low levels of target gene expression. An interesting future question is what is driving
475 NHR-23-depleted animals to eventually attempt to molt? The pre-cuticle component,
476 NOAH-1, and early collagen, ROL-6 are both expressed and secreted but display
477 localization defects. One possibility is that low sustained NHR-23-levels eventually allow
478 the accumulation of factors that initiate apolysis but there is insufficient expression. *nas-*
479 *37* is necessary for *C. elegans* ecdysis and recombinant NAS-37 promotes the formation
480 of retractile rings, a structure associated with molting, in the parasitic nematode *H.*
481 *contortus* (Davis et al., 2004). Another non-exclusionary possibility is that NHR-23
482 controls the expression of transcription factors in a regulatory cascade, similar to the gene
483 regulatory network controlling insect molting (King-Jones and Thummel, 2005; Thummel,
484 1990). *nhr-23* regulates *peb-1* and *dpy-20*, transcription factors with known roles in
485 molting (Clark et al., 1995, 20; Fernandez et al., 2004, 1). *nhr-23* also regulates *nhr-91*
486 (Kouns et al., 2011)(Table S2), a nuclear hormone receptor involved in blast cell
487 progression in response to nutrients (Kasuga et al., 2013). A third possibility is that

488 another timer eventually promotes molting. The molting timer and heterochronic cycles
489 can be uncoupled, causing animals to attempt molting before completion of cell division
490 and differentiation, leading to death (Ruaud and Bessereau, 2006).
491
492 ***nhr-23* is necessary in seam and hypodermal cells to promote molting**
493 When we performed *SCMp*-specific *nhr-23* RNAi, we observed severe developmental
494 delay and molting defects (Fig 8). Hypodermal-specific *nhr-23* knock-down produced less
495 penetrant phenotypes (Fig. 8). The most severe defects in ROL-6 and NOAH-1
496 localization occur above the seam cells (Figure 6). This observation combined with the
497 tissue-specific RNAi data suggests that NHR-23 may be necessary in seam cells for
498 molting, though we cannot rule out an additional role in the hypodermis. However, we
499 observed reduced expression and patchy cuticular localization following NHR-23
500 depletion (Fig. 6), suggesting either that NHR-23 functions in the hypodermis to regulate
501 BLI-1 expression or it is acting cell non-autonomously in the seam cells. Determining how
502 NHR-23 regulates BLI-1 expression and formation of struts will provide insight into aECM
503 assembly. *nhr-23* is expressed in other epidermal cells that produce pre-cuticle and
504 cuticle, such as vulval precursor cells, rectal cells, and excretory duct cells. NHR-23
505 depletion did not produce obvious defects in localization of the pre-cuticle component
506 NOAH-1 in these cells (Fig 6). We did not see phenotypes such as excretory duct or pore
507 lumen dilations, which would be indicative of excretory system defects (Gill et al., 2016).
508 We observed vulval morphology defects following NHR-23 depletion, but it is not clear
509 whether that is due to NHR-23 regulation of this specialized aECM or if it is the
510 consequence of developmental delay and failure to molt. Tissue-specific RNAi or protein
511 depletion will be required to determine whether NHR-23 activity is necessary in these
512 epithelial cells, or if it predominantly functions in seam and hypodermal cells.
513
514 **Future perspectives**
515 This work highlights the power of timed protein depletion for dissecting the role of
516 oscillating developmental regulators in development. As transcription factors coordinate
517 the expression of batteries of genes in a given biological process, future work will reveal
518 how NHR-23 coordinates apical ECM remodeling, apolysis, and ecdysis. NHR-23

519 oscillates in the soma yet is constitutively expressed in the germline (Ragle et al., 2020).
520 Exploring the differences between oscillatory and constitutive NHR-23 expression could
521 shed light on mammalian gene regulation, as several circadian rhythm regulators oscillate
522 in the soma but are constitutively expressed in the testes (Alvarez et al., 2008; Kang et
523 al., 2010; Kennaway et al., 2012; Morse et al., 2003).
524

525 **MATERIALS AND METHODS**

526 ***C. elegans* Strains and Culture**

527 *C. elegans* strains were cultured as originally described (Brenner, 1974), except worms
528 were grown on MYOB instead of NGM. MYOB was made as previously described
529 (Church et al., 1995). Animals were cultured at 20ºC for all assays, unless otherwise
530 indicated. For general strain propagation, animals were grown at 15ºC according to
531 standard protocols. Brood sizes were performed picking L4 larvae to individual wells of a
532 6-well plate seeded with OP50 and incubating the plate at 20ºC. Animals were transferred
533 to new plates daily over 4 days. Two days post-transfer, the number of hatched progeny
534 and unfertilized eggs were scored.
535

536 **Strains used in this study:**

Strain	Construction	Genotype
JDW180	Microinjection	*wrdEx12[SCMp::NLS-mScarlet (dpi)-tbb-2 3'UTR + pCFJ90 (myo-2p::mCherry)]*
JDW258	Ashley *et al.,* 2021	*wrdSi22 [eft-3p::TIR1::F2A::mTagBFP2::AID*::NLS::tbb-2 3'UTR+SEC, I:-5.32] ; nhr-23(kry61(nhr-23::AID*-TEV-3xFLAG)) I*
JDW259	Ashley *et al.,* 2021	*wrdSi55[eft-3p::TIR1::F2A::mTagBFP2::AID*::NLS::tbb-2 3'UTR, I:-5.32] ; nhr-23(kry61(nhr-23::AID*-TEV-3xFLAG)) I*
JDW322	Microinjection	*wrdEx29[wrt-2p::NLS-mScarlet (dpi)-tbb-2 3'UTR]*
JDW348	Crossing	*ieSi57 [Peft-3::TIR1::mRuby::unc-54 3'UTR, cb-unc-119(+?)] II; frIs7 [nlp-29p::GFP + col-12p::DsRed] IV*

JDW349	Crossing	*nhr-23(kry61(nhr-23::AID*-TEV-3xFLAG))I; ieSi57 [Peft-3::TIR1::mRuby::unc-54 3'UTR, cb-unc-119(+?)] II; frIs7 [nlp-29p::GFP + col-12p::DsRed] IV.x*
JDW330	Crossing	*rde-1 (ne300) V.; jsTi1493 [mosL loxP mex-5p FLP sl2 mNeonGreen rpl-28p FRT GFP-HIS-58 FRT3 mosR] IV*
JDW354	Crossing	*wrdSi60[eft-3p::TIR1::F2A::mTagBFP2::AID*::NLS::tbb-2:tbb-2 3'UTR, I:-5.32] I; ayIs6 [hlh-8::GFP fusion + dpy-20(+)] X*
JDW355	Crossing	*wrdSi61[eft-3p::TIR1::F2A::mTagBFP2::AID*::NLS::tbb-2:tbb-2 3'UTR, I:-5.32] ; nhr-23(kry61(nhr-23::AID*-TEV-3xFLAG)) I; ayIs6 [hlh-8::GFP fusion + dpy-20(+)] X*
JDW356	Crossing	*wrdSi59[eft-3p::TIR1::F2A::mTagBFP2::AID*::NLS::tbb-2 3'UTR, I:-5.32], daf-16(mu86) I; ayIs6 [hlh-8::GFP fusion + dpy-20(+)] X*
JDW357	Crossing	*wrdSi59[eft-3p::TIR1::F2A::mTagBFP2::AID*::NLS::tbb-2 3'UTR, I:-5.32], nhr-23(kry61(nhr-23::AID*-TEV-3xFLAG)), daf-16(mu86) I; ayIs6 [hlh-8::GFP fusion + dpy-20(+)] X*
JDW370	Microinjection	*jsTi1493 {mosL::loxP::mex-5p::FLP::sl2::mNeonGreen::rpl-28p::FRT [wrdSi64**(SEC::loxP::SCMp::rde-1 CDS+3'UTR)**] FRT3::mosR} IV ; rde-1 (ne300) V*
JDW371	SEC excision of JDW370	*jsTi1493 {mosL loxP [wrdSi65(SCM**p::rde-1 CDS+3'UTR**)] FRT3::mosR} IV ; rde-1 (ne300) V*
JDW395	Crossing	*wrdSi73[eft-3p::TIR1::F2A::mTagBFP2::AID*::NLS::tbb-2 3'UTR] ; nhr-23(kry61(nhr-23::AID*-TEV-3xFLAG)) I; oxIs134[Pnas-37::GFP:rODC(pest)(pWD95@90ng/ul),lin-15(+)]*
JDW459	Microinjection	*nhr-23(kry61(nhr-23::AID*-TEV-3xFLAG))I; ieSi57 [Peft-3::TIR1::mRuby::unc-54 3'UTR, cb-unc-119(+?)] II*
JDW463	Microinjection	*nhr-23(kry61(nhr-23::AID*-TEV-3xFLAG)) I ; ieSi57 [Peft-3::TIR1::mRuby::unc-54 3'UTR, cb-unc-119(+?)] , bli-1(wrd122[bli-1::internal mNeonGreen (dpi)::3xFLAG::linker]) II*
JDW472	Microinjection	*rol-6(wrd123[rol-6::C-term mNeonGreen (dpi)::3xFLAG::linker]) I ; jsTi1493 wrdSi65[SCMmin::pes-10delta::rde-1 CDS+3'UTR in pLF3FShC]IV; rde-1(ne300) V.*

JDW475	Microinjection	*noah-1(wrd126[noah-1::internal mNeonGreen (dpi)::3xFLAG::linker]) , nhr-23(kry61(nhr-23::AID*-TEV-3xFLAG)) I ; ieSi57 [Peft-3::TIR1::mRuby::unc-54 3'UTR, cb-unc-119(+?)] II*
JDW509	Microinjection	*jsTi1493 {mosL::loxP::mex-5p::FLP::sl2::mNeonGreen::rpl-28p::FRT [wrdSi96**(SEC::loxP::semo-1 (Y37A1B.5)p::rde-1 CDS+3'UTR)**] FRT3::mosR} IV ; rde-1 (ne300) V*
JDW510	SEC excision of JDW509	*jsTi1493 {mosL loxP [wrdSi97(**semo-1p::rde-1 CDS+3'UTR**)] FRT3::mosR} IV ; rde-1 (ne300) V*
JDW525	Microinjection	*his-72(wrd142[mNeonGreen::his-72]) III ; jsTi1493 {mosL loxP [wrdSi65(SCMp::rde-1 CDS+3'UTR)] FRT3::mosR} IV ; rde-1 (ne300) V*
KRY87	(Zhang et al., 2015)	*nhr-23(kry61(nhr-23::AID*-TEV-3xFLAG))I*
KRY88	Zhang et al., 2015	*nhr-23(kry61(nhr-23::AID*-TEV-3xFLAG))I; ieSi57 [Peft-3::TIR1::mRuby::unc-54 3'UTR, cb-unc-119(+?)] II*
NM5179	Nonet, 2020	*jsTi1493 [mosL loxP mex-5p FLP sl2 mNeonGreen rpl-28p FRT GFP-HIS-58 FRT3 mosR] IV*

537

538 Strains provided by the *Caenorhabditis* Genetics Center:
539

Strain	**Genotype**
N2	Wild-type
CA1200	*ieSi57 [Peft-3::TIR1::mRuby::unc-54 3'UTR, cb-unc-119 (+?)] II* (Zhang *et al.,* 2015)
CF1038	*daf-16(mu86) I* *(Lin et al., 1997)*
PD4666	*ayIs6 [hlh-8::GFP fusion + dpy-20(+)] X (Harfe et al., 1998)*

QK52	*rde-1(ne219) V ;* *xkIs99(wrt-2p::rde-1::unc-54 3'UTR) (Melo and Ruvkun, 2012)*
VP303	*rde-1(ne219) V ;* *kbIs7[nhx-2p::rde-1 + rol-6(su1006)]) (Espelt et al., 2005)*
JU2039	*mfIs70* *[lin-31p::rde-1 + myo2p::GFP] IV ; rde-1(ne219) V (Barkoulas et al., 2013)*
WM118	*rde-1(ne300) V ; neIs9(neIs9 [myo-3::HA::RDE-1 + rol-6(su1006)]) X* (Watts et al., 2020)
MGH171	*alxIs9 [vha-6p::sid-1::SL2::GFP] sid-1(qt9) V (Melo and Ruvkun, 2012)*
NM5179	*jsTi1493 [mosL loxP mex-5p FLP sl2 mNeonGreen rpl-28p FRT GFP-HIS-58 FRT3 mosR] IV (Nonet, 2020)*
WM45	*rde-1(ne300) V* (Tabara et al., 1999)
IG274	*frIs7 [nlp-29p::GFP + col-12p::DsRed] IV* (Pujol et al., 2008)

Other strains

EG3200 *oxIs134[Pnas-37::GFP:rODC (pest) (pWD95@90ng/ul),lin-15(+)]; lin-15(n765ts)* X (Davis et al., 2004) was provided by D. Fay (U Wyoming).

Genome editing and transgenesis

mNeonGreen::3xFLAG knock-ins into *bli-1, noah-1,* and *rol-6* and *mNeonGreen* knock-ins into *his-72* were generated by injection of Cas9 ribonucleoprotein complexes [700 ng/ul IDT Cas9, 115 ng/ul crRNA and 250 ng/ul IDT tracrRNA] and a dsDNA repair template (25-50 ng/ul) created by PCR amplification of a plasmid template (Paix et al., 2014; Paix et al., 2015). The PCR products were melted to boost editing efficiency, as previously described (Ghanta and Mello, 2020). crRNAs used are provided in Table S6. Oligonucleotides used for repair template generation from template pJW2172 (Ashley et al., 2021) and for genotyping are provided in Table S7. Genomic and knock-in sequences are provided in File S1. Plasmids used are provided in Table S8. To generate JDW371 and JDW510 (seam cell and hypodermal-specific tissue-specific RNAi) we crossed a

556 *jsTi1493* landing pad for recombination-mediated cassette exchange (RMCE)(Nonet,
557 2020) into an *rde-1(ne300*) null mutant, generating JDW330. We used GIbson cloning to
558 introduce a promoterless *rde-1* genomic coding sequence+3'UTR fragment into the
559 RMCE integration vector pLF3FShC (Nonet, 2020), creating pJW2247. This vector can
560 be linearized with *Avr*II+*Bsi*WI double-digestion and promoters can be introduced by
561 Gibson cloning (Gibson et al., 2009). We generated a *SCMp* (seam cell-specific) and
562 *semo-1p* (hypodermis specific) by Gibson cloning promoters into linearized pJW2247,
563 constructing pJW2236 and pJW2264, respectively. These vectors were integrated into
564 *jsTi1493* landing pad in JDW330 using RMCE, as described (Nonet, 2020). *wrt-2p* and
565 *SCMp* promoter reporters were constructed in pJW1836 (*NLS::mScarlet::tbb-2 3'*
566 *UTR*)(Ashley et al., 2021) by Gibson cloning. Plasmids were injected into N2 animals at
567 50 ng/µl with a pCFJ90 co-injection marker at 10 ng/µl for the *SCMp* promoter reporter
568 and a pRF4 co-injection marker at 50 ng/µl for the *wrt-2* promoter reporter (Frøkjaer-
569 Jensen et al., 2008; Mello et al., 1991). Transgenic lines propagating extrachromosomal
570 arrays were generated as previously described (Mello et al., 1991). Sequence files for
571 plasmids are provided in File S2. Primers and cloning details are available upon request.
572

573 **Auxin treatment**

574 Control and auxin media/plates were made as described in Ragle et al. 2020. Control
575 media consisted of MYOB agar+0.25% ethanol. Auxin media was made by dissolving
576 indole 3-acetic acid (IAA; Alfa Aesar, AAA1055622) in 100% ethanol to 1.6 M and then
577 mixing it into melted MYOB agar at 55°C to a final concentration of 4 mM prior to pouring
578 plates. Control plates contained 0.25 % ethanol. Temperature of the media was monitored
579 with a Lasergrip 1080 infrared thermometer gun (Etekcity). Plates were seeded with *E.*
580 *coli* OP50 and incubated overnight at room temperature. Plates were stored for up to one
581 month at 4ºC prior to use. For most auxin treatment experiments, animals were
582 synchronized by alkaline bleaching (dx.doi.org/10.17504/protocols.io.j8nlkkyxdl5r/v1).
583 The collected eggs were incubated in M9 buffer supplemented with 5 mg/mL cholesterol
584 at 20ºC for 24 hours and arrested L1 larvae were released onto the indicated type of
585 MYOB plate. For the experiment in Table S1 a timed egg lay was performed. Twenty adult
586 hermaphrodites animals of the indicated genotype were picked onto control (0.25%

587 ethanol) or auxin (4 mM IAA) plates and allowed to lay eggs for 2 hours. The adult animals
588 were removed and plates were incubated for 48 hours at 25ºC.
589
590 **Microscopy**
591 Synchronized animals were collected from MYOB, control, or auxin plates by either
592 picking or washing off plates. For washing, 1000 µl of M9 + 0.05% gelatin was added to
593 the plate or well, agitated to suspend animals in M9+gelatin, and then transferred to a 1.5
594 ml tube. Animals were spun at 700xg for 1 min. The media was then aspirated off and
595 animals were resuspended in 500µl M9 + 0.05% gelatin with 5 mM levamisole. 12 µl of
596 animals in M9 + 0.05% with levamisole solution were placed on slides with a 2% agarose
597 pad and secured with a coverslip. For picking, animals were transferred to a 10 µl drop of
598 M9+5 mM levamisole on a 2% agarose pad on a slide and secured with a coverslip.
599 Images were acquired using a Plan-Apochromat 40x/1.3 Oil DIC lens or a Plan-
600 Apochromat 63x/1.4 Oil DIC lens on an AxioImager M2 microscope (Carl Zeiss
601 Microscopy, LLC) equipped with a Colibri 7 LED light source and an Axiocam 506 mono
602 camera. Acquired images were processed through Fiji software (version: 2.0.0- rc-
603 69/1.52p). For direct comparisons within a figure, we set the exposure conditions to avoid
604 pixel saturation of the brightest sample and kept equivalent exposure for imaging of the
605 other samples.
606
607 **Phenotypic analysis**
608 For the phenotypic analysis in Figure 2, synchronized CA1200 or KRY88 larvae were
609 released onto MYOB plates and then shifted onto control or auxin plates every two hours
610 up to 16 hours. Animals were collected as described in the Microscopy section and
611 imaged by DIC microscopy to score for morphology and shedding of the L1 cuticles. For
612 the M cell lineage experiments in Figures S5, synchronized animals of the indicated
613 genotypes were released onto MYOB plates and shifted onto control or auxin plates at 3
614 hours (early shift) or 9 hours (late shift) post-release and then imaged at 24 hours post-
615 release, as described in the Microscopy section. M cells were counted and recorded. For
616 the L3 shift experiments (Fig. 3A-D) synchronized animals of the indicated genotype were
617 grown on MYOB. At 25 hours post-release, they were shifted onto 6-well control or auxin

618 MYOB plates seeded with OP50. 24, 48, or 72 hours later animals were collected as
619 described in the Microscopy section and imaged by DIC microscopy using a 63x lens to
620 stage animals according to vulval morphology (Mok et al., 2015). For the analyses in
621 Figure 3E-F, synchronized *nhr-23::AID, TIR1* larvae were released on auxin plates and
622 scored for viability and molting defects 48 and 72 hours later. For the reporter timecourse,
623 synchronized *nhr-23::AID, TIR1, nas-37p::GFP::PEST* animals were released on control
624 or auxin plates. They were then scored for GFP expression using a PlanApo 5.0x/0.5
625 objective on a M165 FC stereomicroscope (Leica) equipped with an X-cite FIRE LED
626 lightsource (Excelitas) and long pass GFP filter set (Leica #10447407). We scored GFP
627 expression in the head and hypodermis and did not score rectal GFP expression, as
628 expression perdured in this tissue after head and hypodermal GFP expression ceased.
629
630 **Barrier assays**
631 Hoechst 33258 staining was performed as described previously (Moribe et al., 2004),
632 except that we used 10 µg/ml of Hoechst 33258 as in Ward et al. (2014). Two biological
633 replicates were performed examining 50 animals per experiment. The number of animals
634 with either head or hypodermal nuclei staining with Hoechst 33258 were scored under a
635 10x DIC objective. Representative images were then taken with equivalent exposures
636 using a 63x Oil DIC lens, as described in the imaging section. Hypo-osmotic stress
637 sensitivity assays were performed on L4 stage larvae as described (Ward et al., 2014),
638 except we used 20µl of dH_20. Each strain was assayed in triplicate.
639
640 **Western Blots**
641 Animals were synchronized by alkaline bleaching, as described in the “Auxin Treatment”
642 section. For the blot in Fig. S6B, 30 animals of the indicated genotype and stage were
643 picked into 30 µl of M9+0.05% gelatin and 10 µl of 4x Laemmli sample buffer was added
644 and then samples were heated at 95ºC for 5 minutes and stored at -80ºC until they were
645 resolved by SDS-PAGE (described in following paragraph). For the blot in Fig. S6B,
646 ~1000 animals of the indicated genotype were washed out of a 6 cm MYOB plate,
647 transferred to a 1.5 ml tube and washed twice more with M9+0.05% gelatin, as previously
648 described (Vo et al., 2021). Animals were pelleted and flash frozen in 50 µl of M9+gelatin

649 in liquid nitrogen. Samples were stored at -80ºC. Lysates were made by adding 50 µl of
650 2xRIPA buffer (Sigma SIAL-20-188) supplemented with 2 mM PMSF and Protease
651 Inhibitor Cocktail Set III, EDTA-Free (Calbiochem #539134) and sonicating in a
652 Diagenode Bioruptor for 30 cycles of 30 seconds on/30 seconds off. Laemmli sample
653 buffer was added to 1X and samples were heated at 70ºX for 10 minutes to denature the
654 protein. For the remaining blots, animals of the indicated genotype were washed out of
655 wells on a 6-well plate at the indicated timepoints with M9+0.05% gelatin (VWR, 97062-
656 620), transferred to a 1.5 ml tube and washed twice more with M9+0.05% gelatin, as
657 previously described (Vo et al., 2021). Animals were pelleted, transferred in a 100 µl
658 volume to a new 1.5 ml tube, and flash frozen in liquid nitrogen, then stored at -80ºC.
659 Prior to SDS-PAGE, samples were freeze-cracked twice in liquid nitrogen or on dry ice,
660 Laemmli sample buffer was added to 1X and samples were heated to 95ºC for 5 minutes.
661 For the western blots in Figure 1C 6000 KRY88 animals per well were transferred onto a
662 6-well MYOB plate seeded with OP50. For the western blot in Figure 2B, 6000
663 synchronized KRY88 animals were plated onto control or auxin plates. Control animals
664 were harvested at peak NHR-23 expression (12 hours of growth on control plates) and
665 auxin-treated animals were shifted onto auxin at this time and samples were taken at the
666 indicated time points, as described above. For the western blots in Figure 7C, 500 animals
667 of the indicated genotype were transferred into wells of a 6-well control or auxin plate
668 seeded with OP50. Animals were incubated for 24 hours at 20ºC and collected as
669 described above.
670
671 For the blots in Figs. 1C, 10 µl of lysate and 7.5 µl 1:1 mix of Amersham ECL Rainbow
672 Molecular Weight Markers (95040-114) and Precision Plus Protein Unstained Standards
673 (#1610363) was resolved by SDS-PAGE using precast 4-20% MiniProtean TGX Stain
674 Free Gels (Bio-Rad). The blot in Fig. 7C, the lysates had more variable levels of total
675 protein, particularly the NHR-23 depleted samples that produced an early larval arrest.
676 Therefore we quantified the signal of the most intense band by Stain Free imaging (Posch
677 et al., 2013) using a Bio-Rad ChemiDoc imaging system, and ran a new gel with
678 normalized loading. The lysates in Fig. 2B, 7C, S6B and C were resolved as described
679 adobe except we used a Spectra™ Multicolor Broad Range Protein Ladder (Thermo; #

680 26623). Proteins were transferred to a polyvinylidene difluoride membrane by semi-dry
681 transfer with a TransBlot Turbo (Bio-Rad). In Figs 1C and 7C, total protein, pre- and post-
682 transfer, was monitored using the stain-free fluorophore as described (Posch et al., 2013;
683 Ward, 2015a). Membranes were washed in TBST and blocked in TBST+5% milk (TBST-
684 M; Nestle Carnation Instant Nonfat Dry Milk, 25.6-Ounce, Amazon) for one hour at room
685 temperature. Blots were rocked in primary antibodies in TBST-M overnight at 4ºC and
686 then washed 4x5min with TBST. For primary antibodies conjugated with horseradish
687 peroxidase (HRP) the blots were developed after the last TBST wash. Otherwise, blots
688 were incubated with HRP-conjugated secondary antibodies in TBST-M for one hour at
689 room temperature followed by 4x5min TBST washes and then developed as described
690 below.
691
692 The primary antibody used for Figures 1C, 2B, and S6B and C was horseradish
693 peroxidase (HRP) conjugated anti-FLAG M2 (Sigma-Aldrich, A8592-5x1MG, Lot
694 #SLCB9703) at a 1:2000 dilution. Precision Protein StrepTactin-HRP Conjugate (Bio-
695 Rad, #1610381, Lot #64426657) was included with the primary antibody at a 1:10,000
696 dilution to visualize the protein size standard during blot imaging for Figs 1C. For the blot
697 in Fig. 2B, 7C, 6B and C, we used mouse anti-alpha-Tubulin 12G10 (Developmental
698 Studies Hybridoma Bank, the "-c" concentrated supernatant at 1:2000 (Fig 7C, 2B) or
699 1:4000 (Fig. S6B,C). The secondary antibodies were Digital anti-mouse (Kindle
700 Biosciences LLC, R1005) diluted 1:10,000 (Fig. 2B, 7C) or 1:20,000 (Fig. S6B,C). Blots
701 were incubated for 5 minutes with 1 ml of Supersignal West Femto Maximum Sensitivity
702 Substrate (Thermo Fisher Scientific, 34095) and imaged using the 'chemi high-resolution'
703 setting on a Bio-Rad ChemiDoc MP System.
704
705 **Bioinformatics**
706 Figure 4A was generated in R (R Core Team). Phase and amplitude in Table S2 were
707 converted to x and y coordinates for each gene by calculating x = amplitude * cos(phase)
708 and y = amplitude * sin(phase). For Figure 4B and S5, L3 NHR-23 ChIP-Seq data was
709 downloaded from http://www.modencode.org, accession ID modEncode_3837. Wig files
710 were converted to bigwig format and loaded into the Bioconductor package SeqPlots

711 (cite_SeqPlots)(Huber et al., 2015; Stempor and Ahringer, 2016). A bed file with the start
712 and end coordinates of all genes' CDS was generated and loaded into SeqPlots. SeqPlots
713 aligned all genes by the start and end position and scaled the coding sequence of each
714 gene to 2 kb. The average signal over all aligned genes was calculated in 25 bp windows
715 from 1 kb upstream of the start site to 1kb downstream of the end site. Peak calls for
716 NHR-23 in L3 (Fig 4C) were obtained from GEO (accession numbers: GSM1183659,
717 GSM1183660, GSM1183661, GSM118366)Only peak calls validated by both replicates
718 were considered. Peaks were assigned to the following genome features: gene body
719 (WormBase WS220), 1kb upstream of the start site of coding genes, between 1kb and
720 3kb upstream of the gene start site and between 3kb and 5kb upstream of the gene start
721 site. The same intervals were chosen downstream of the gene end sites. A NHR-23 peak
722 was assigned to a feature if it overlapped with it by at least 100bp. The peak analysis data
723 is in Table S5. The total number of peaks in all bins was tallied and is presented in Table
724 S2 and in Figure 4C. For Fig. 4D and 4E the phase for the oscillating genes in Table S1
725 was converted to time during the molting cycle by assuming a 9 hour larval stage which
726 makes each hour=40º. The phase in hours was then plotted along the x axis and the
727 oscillating genes' amplitude was plotted on the y axis. The gene annotation was based
728 on the Concise Description and Automated Description downloaded from Wormbase.
729
730 **RNAi**
731 RNAi feeding plates were made by melting a solidified bottle of MYOB and adding
732 Carbenicillin (25 ug/ml) and IPTG (8mM) once cooled to 55℃. dsRNA-expressing *E. coli*
733 bacteria were streaked on LB plates with Ampicillin (100 µg/ml) and grown overnight at
734 37℃. A single colony was picked into 25 ml LB with 100 µg/ml Ampicillin and 12.5 µg/ml
735 Tetracycline and shaken overnight at 37℃ at 220 RPMs. The next day, the liquid culture
736 was pelleted and resuspended in 1.25 ml LB with 100 µg/ml Ampicillin resulting in a 20x
737 concentration from the original overnight liquid culture. 90 µl of the liquid culture was
738 spread per small RNAi plate and allowed to dry. The plates were incubated at room
739 temperature in the dark for 3 days. 10 adult worms from each strain were allowed to lay
740 eggs on plates spread with *E. coli* bacteria containing either the control plasmid L4440 or

741 the *nhr-23* RNAi knockdown plasmid for 1-2 hours. The adults were removed and the
742 eggs allowed to develop at 20℃ for 2 or 3 days depending on the experiment.
743
744 **Statistical Analysis**
745 Statistical tests and numbers of animals analyzed are detailed in figure legends.
746
747 **Competing interests**
748 The authors declare no competing or financial interests.
749
750
751 **Acknowledgements**
752 We thank Chris Hammell, David Matus, and Julian Ceron Madrigal for their critical reading
753 of the manuscript. We thank David Fay, Miles Pufall, Helge Grosshans, and Ali Shariati
754 for helpful discussions. We thank Andrew Chisholm and Jennifer Adams for providing
755 information about *rol-6* and *bli-1* mNeonGreen knock-ins that they generated. Figure 1A
756 and S4A were created with Biorender.com.
757
758 **Funding**
759 This work was funded by the National Institutes of Health (NIH) National Institute
760 of General Medical Sciences (NIGMS) [R00GM107345 and R01 GM138701] to J.D.W.
761 Some strains were provided by the Caenorhabditis Genetics Center, which is funded by
762 the NIH Office of Research Infrastructure Programs [P40 OD010440]. L.C.J. was funded
763 by an NIGMS training grant [T32 GM133391]. The anti-alpha tubulin 12G10 monoclonal
764 antibody developed by J. Frankel and E.M. Nelson of the University of Iowa was obtained
765 from the Developmental Studies Hybridoma Bank, created by the NICHD of the NIH and
766 maintained at The University of Iowa, Department of Biology, Iowa City, IA 52242.
767

768 **REFERENCES**

769 **Agbulut, O., Coirault, C., Niederländer, N., Huet, A., Vicart, P., Hagège, A., Puceat,**
770 **M. and Menasché, P.** (2006). GFP expression in muscle cells impairs actin-

771 myosin interactions: implications for cell therapy. *Nat. Methods* **3**, 331–331.
772 **Alvarez, J. D., Hansen, A., Ord, T., Bebas, P., Chappell, P. E., Giebultowicz, J. M.,**
773 **Williams, C., Moss, S. and Sehgal, A.** (2008). The circadian clock protein
774 BMAL1 is necessary for fertility and proper testosterone production in mice. *J.*
775 *Biol. Rhythms* **23**, 26–36.
776 **Antebi, A.** (2015). Nuclear receptor signal transduction in *C. elegans*. *WormBook* 1–49.
777 **Ashley, G. E., Duong, T., Levenson, M. T., Martinez, M. A. Q., Johnson, L. C.,**
778 **Hibshman, J. D., Saeger, H. N., Palmisano, N. J., Doonan, R., Martinez-**
779 **Mendez, R., et al.** (2021). An expanded auxin-inducible degron toolkit for
780 *Caenorhabditis elegans*. *Genetics* **217**, iyab006.
781 **Aspöck, G., Kagoshima, H., Niklaus, G. and Bürglin, T. R.** (1999). *Caenorhabditis*
782 *elegans* has scores of hedgehog-related genes: sequence and expression
783 analysis. *Genome Res.* **9**, 909–923.
784 **Baens, M., Noels, H., Broeckx, V., Hagens, S., Fevery, S., Billiau, A. D.,**
785 **Vankelecom, H. and Marynen, P.** (2006). The Dark Side of EGFP: Defective
786 Polyubiquitination. *PLOS ONE* **1**, e54.
787 **Barkoulas, M., van Zon, J. S., Milloz, J., Van Oudenaarden, A. and Félix, M.-A.**
788 (2013). Robustness and Epistasis in the *C. elegans* Vulval Signaling Network
789 Revealed by Pathway Dosage Modulation. *Dev. Cell* **24**, 64–75.
790 **Baugh, L. R. and Sternberg, P. W.** (2006). DAF-16/FOXO regulates transcription of
791 *cki-1*/Cip/Kip and repression of *lin-4* during *C. elegans* L1 arrest. *Curr. Biol.* **16**,
792 780–785.
793 **Blaxter, M. L.** (1993). Cuticle surface proteins of wild type and mutant *Caenorhabditis*
794 *elegans*. *J. Biol. Chem.* **268**, 6600–6609.
795 **Blaxter, M. L., Page, A. P., Rudin, W. and Maizels, R. M.** (1992). Nematode surface
796 coats: actively evading immunity. *Parasitol. Today Pers. Ed* **8**, 243–247.
797 **Brenner, S.** (1974). The genetics of *Caenorhabditis elegans*. *Genetics* **77**, 71–94.
798 **Campbell, L. A., Faivre, E. J., Show, M. D., Ingraham, J. G., Flinders, J., Gross, J.**
799 **D. and Ingraham, H. A.** (2008). Decreased Recognition of SUMO-Sensitive
800 Target Genes following Modification of SF-1 (NR5A1). *Mol. Cell. Biol.* **28**, 7476–
801 7486.

802 **Church, D. L., Guan, K. L. and Lambie, E. J.** (1995). Three genes of the MAP kinase
803 cascade, *mek-2*, *mpk-1/sur-1* and *let-60 ras*, are required for meiotic cell cycle
804 progression in *Caenorhabditis elegans*. *Development* **121**, 2525–2535.
805 **Clark, D. V., Suleman, D. S., Beckenbach, K. A., Gilchrist, E. J. and Baillie, D. L.**
806 (1995). Molecular cloning and characterization of the *dpy-20* gene of
807 *Caenorhabditis elegans*. *Mol. Gen. Genet. MGG* **247**, 367–378.
808 **Cohen, J. D. and Sundaram, M. V.** (2020). *C. elegans* Apical Extracellular Matrices
809 Shape Epithelia. *J. Dev. Biol.* **8**, 23.
810 **Cohen, J. D., Sparacio, A. P., Belfi, A. C., Forman-Rubinsky, R., Hall, D. H., Maul-**
811 **Newby, H., Frand, A. R. and Sundaram, M. V.** (2020). A multi-layered and
812 dynamic apical extracellular matrix shapes the vulva lumen in *Caenorhabditis*
813 *elegans*. *eLife* **9**, e57874.
814 **Davis, M. W., Birnie, A. J., Chan, A. C., Page, A. P. and Jorgensen, E. M.** (2004). A
815 conserved metalloprotease mediates ecdysis in *Caenorhabditis elegans*.
816 *Development* **131**, 6001–6008.
817 **de Sousa Abreu, R., Penalva, L. O., Marcotte, E. M. and Vogel, C.** (2009). Global
818 signatures of protein and mRNA expression levels. *Mol. Biosyst.* **5**, 1512–1526.
819 **Dodd, W., Tang, L., Lone, J.-C., Wimberly, K., Wu, C.-W., Consalvo, C., Wright, J.**
820 **E., Pujol, N. and Choe, K. P.** (2018). A Damage Sensor Associated with the
821 Cuticle Coordinates Three Core Environmental Stress Responses in
822 *Caenorhabditis elegans*. *Genetics* **208**, 1467–1482.
823 **Espelt, M. V., Estevez, A. Y., Yin, X. and Strange, K.** (2005). Oscillatory Ca2+
824 signaling in the isolated *Caenorhabditis elegans* intestine: role of the inositol-
825 1,4,5-trisphosphate receptor and phospholipases C beta and gamma. *J. Gen.*
826 *Physiol.* **126**, 379–392.
827 **Fernandez, A. P., Gibbons, J. and Okkema, P. G.** (2004). *C. elegans peb-1* mutants
828 exhibit pleiotropic defects in molting, feeding, and morphology. *Dev. Biol.* **276**,
829 352–366.
830 **Fielenbach, N. and Antebi, A.** (2008). *C. elegans* dauer formation and the molecular
831 basis of plasticity. *Genes Dev.* **22**, 2149–2165.
832 **Forman-Rubinsky, R., Cohen, J. D. and Sundaram, M. V.** (2017). Lipocalins Are

833 Required for Apical Extracellular Matrix Organization and Remodeling in
834 *Caenorhabditis elegans*. *Genetics* **207**, 625–642.
835 **Frand, A. R., Russel, S. and Ruvkun, G.** (2005). Functional Genomic Analysis of *C.*
836 *elegans* Molting. *PLoS Biol.* **3**, e312.
837 **Frøkjaer-Jensen, C., Davis, M. W., Hopkins, C. E., Newman, B. J., Thummel, J. M.,**
838 **Olesen, S.-P., Grunnet, M. and Jorgensen, E. M.** (2008). Single-copy insertion
839 of transgenes in *Caenorhabditis elegans*. *Nat. Genet.* **40**, 1375–1383.
840 **Gerstein, M. B., Lu, Z. J., Van Nostrand, E. L., Cheng, C., Arshinoff, B. I., Liu, T.,**
841 **Yip, K. Y., Robilotto, R., Rechtsteiner, A., Ikegami, K., et al.** (2010).
842 Integrative Analysis of the *Caenorhabditis elegans* Genome by the modENCODE
843 Project. *Science* **330**, 1775–1787.
844 **Ghanta, K. S. and Mello, C. C.** (2020). Melting dsDNA Donor Molecules Greatly
845 Improves Precision Genome Editing in *Caenorhabditis elegans*. *Genetics* **216**,
846 643–650.
847 **Ghedin, E., Wang, S., Spiro, D., Caler, E., Zhao, Q., Crabtree, J., Allen, J. E.,**
848 **Delcher, A. L., Guiliano, D. B., Miranda-Saavedra, D., et al.** (2007). Draft
849 genome of the filarial nematode parasite *Brugia malayi*. *Science* **317**, 1756–
850 1760.
851 **Gibson, D. G., Young, L., Chuang, R.-Y., Venter, J. C., Hutchison, C. A. and Smith,**
852 **H. O.** (2009). Enzymatic assembly of DNA molecules up to several hundred
853 kilobases. *Nat. Methods* **6**, 343–345.
854 **Gill, H. K., Cohen, J. D., Ayala-Figueroa, J., Forman-Rubinsky, R., Poggioli, C.,**
855 **Bickard, K., Parry, J. M., Pu, P., Hall, D. H. and Sundaram, M. V.** (2016).
856 Integrity of Narrow Epithelial Tubes in the C. elegans Excretory System Requires
857 a Transient Luminal Matrix. *PLoS Genet.* **12**, e1006205.
858 **Gissendanner, C. R., Crossgrove, K., Kraus, K. A., Maina, C. V. and Sluder, A. E.**
859 (2004). Expression and function of conserved nuclear receptor genes in
860 *Caenorhabditis elegans*. *Dev. Biol.* **266**, 399–416.
861 **Harfe, B. D., Gomes, A. V., Kenyon, C., Liu, J., Krause, M. and Fire, A.** (1998).
862 Analysis of a *Caenorhabditis elegans* Twist homolog identifies conserved and
863 divergent aspects of mesodermal patterning. *Genes Dev.* **12**, 2623–2635.

Hauser, Y. P., Meeuse, M. W. M., Gaidatzis, D. and Großhans, H. (2021). The BLMP-1 transcription factor promotes oscillatory gene expression to achieve timely molting. *bioRxiv* 2021.07.05.450828.

Hendriks, G.-J., Gaidatzis, D., Aeschimann, F. and Großhans, H. (2014). Extensive oscillatory gene expression during *C. elegans* larval development. *Mol. Cell* **53**, 380–392.

Huber, W., Carey, V. J., Gentleman, R., Anders, S., Carlson, M., Carvalho, B. S., Bravo, H. C., Davis, S., Gatto, L., Girke, T., et al. (2015). Orchestrating high-throughput genomic analysis with Bioconductor. *Nat. Methods* **12**, 115–121.

Jetten, A. M. (2009). Retinoid-related orphan receptors (RORs): critical roles in development, immunity, circadian rhythm, and cellular metabolism. *Nucl. Recept. Signal.* **7**,.

Johnstone, I. L. and Barry, J. D. (1996). Temporal reiteration of a precise gene expression pattern during nematode development. *EMBO J.* **15**, 3633–3639.

Kage-Nakadai, E., Kobuna, H., Kimura, M., Gengyo-Ando, K., Inoue, T., Arai, H. and Mitani, S. (2010). Two very long chain fatty acid acyl-CoA synthetase genes, *acs-20* and *acs-22*, have roles in the cuticle surface barrier in *Caenorhabditis elegans*. *PLoS ONE* **5**, e8857.

Kaletsky, R., Yao, V., Williams, A., Runnels, A. M., Tadych, A., Zhou, S., Troyanskaya, O. G. and Murphy, C. T. (2018). Transcriptome analysis of adult *Caenorhabditis elegans* cells reveals tissue-specific gene and isoform expression. *PLOS Genet.* **14**, e1007559.

Kang, T.-H., Lindsey-Boltz, L. A., Reardon, J. T. and Sancar, A. (2010). Circadian control of XPA and excision repair of cisplatin-DNA damage by cryptochrome and HERC2 ubiquitin ligase. *Proc. Natl. Acad. Sci.* **107**, 4890–4895.

Kaplan, R. E. W. and Baugh, L. R. (2016). L1 arrest, *daf-16*/FoxO and nonautonomous control of post-embryonic development. *Worm* **5**, e1175196.

Kasuga, H., Fukuyama, M., Kitazawa, A., Kontani, K. and Katada, T. (2013). The microRNA miR-235 couples blast-cell quiescence to the nutritional state. *Nature* **497**, 503–506.

Kelley, M., Yochem, J., Krieg, M., Calixto, A., Heiman, M. G., Kuzmanov, A., Meli,

895 **V., Chalfie, M., Goodman, M. B., Shaham, S., et al.** (2015). FBN-1, a fibrillin-
896 related protein, is required for resistance of the epidermis to mechanical
897 deformation during *C. elegans* embryogenesis. *eLife* **4**, 1629.
898 **Kennaway, D. J., Boden, M. J. and Varcoe, T. J.** (2012). Circadian rhythms and
899 fertility. *Mol. Cell. Endocrinol.* **349**, 56–61.
900 **Kim, D. hyun, Grün, D. and van Oudenaarden, A.** (2013). Dampening of expression
901 oscillations by synchronous regulation of a microRNA and its target. *Nat. Genet.*
902 **45**, 1337–1344.
903 **King-Jones, K. and Thummel, C. S.** (2005). Nuclear receptors-a perspective from
904 *Drosophila*. *Nat. Rev. Genet.* **6**, 311–323.
905 **Köhnlein, K., Urban, N., Guerrero-Gómez, D., Steinbrenner, H., Urbánek, P.,**
906 **Priebs, J., Koch, P., Kaether, C., Miranda-Vizuete, A. and Klotz, L.-O.** (2020).
907 A *Caenorhabditis elegans* ortholog of human selenium-binding protein 1 is a pro-
908 aging factor protecting against selenite toxicity. *Redox Biol.* **28**, 101323.
909 **Kostrouchova, M., Krause, M., Kostrouch, Z. and Rall, J. E.** (1998). CHR3: a
910 *Caenorhabditis elegans* orphan nuclear hormone receptor required for proper
911 epidermal development and molting. *Development* **125**, 1617–1626.
912 **Kostrouchova, M., Krause, M., Kostrouch, Z. and Rall, J. E.** (2001). Nuclear
913 hormone receptor CHR3 is a critical regulator of all four larval molts of the
914 nematode *Caenorhabditis elegans*. *Proc. Natl. Acad. Sci. U. S. A.* **98**, 7360–
915 7365.
916 **Kouns, N. A., Nakielna, J., Behensky, F., Krause, M. W., Kostrouch, Z. and**
917 **Kostrouchova, M.** (2011). NHR-23 dependent collagen and hedgehog-related
918 genes required for molting. *Biochem. Biophys. Res. Commun.* **413**, 515–520.
919 **Kramer, J. M. and Johnson, J. J.** (1993). Analysis of mutations in the sqt-1 and rol-6
920 collagen genes of Caenorhabditis elegans. *Genetics* **135**, 1035–1045.
921 **Lam, G. T., Jiang, C. and Thummel, C. S.** (1997). Coordination of larval and prepupal
922 gene expression by the DHR3 orphan receptor during *Drosophila*
923 metamorphosis. *Development* **124**, 1757–1769.
924 **Lažetić, V. and Fay, D. S.** (2017). Molting in *C. elegans*. *Worm* **6**, 1–20.
925 **Lin, K., Dorman, J. B., Rodan, A. and Kenyon, C.** (1997). *daf-16*: An HNF-3/forkhead

926 family member that can function to double the life-span of *Caenorhabditis*
927 *elegans*. *Science* **278**, 1319–1322.
928 **Macneil, L. T., Watson, E., Arda, H. E., Zhu, L. J. and Walhout, A. J. M.** (2013). Diet-
929 Induced Developmental Acceleration Independent of TOR and Insulin in *C.*
930 *elegans*. *Cell* **153**, 240–252.
931 **Meeuse, M. W., Hauser, Y. P., Morales Moya, L. J., Hendriks, G., Eglinger, J.,**
932 **Bogaarts, G., Tsiairis, C. and Großhans, H.** (2020). Developmental function
933 and state transitions of a gene expression oscillator in *Caenorhabditis elegans*.
934 *Mol. Syst. Biol.* **16**,.
935 **Meeuse, M. W. M., Nahar, S., Braun, K. and Großhans, H.** (2022). The
936 Grainyhead/LSF transcription factor GRH-1 is rhythmically required for molting.
937 2022.03.01.482504.
938 **Mello, C. C., Kramer, J. M., Stinchcomb, D. and Ambros, V.** (1991). Efficient gene
939 transfer in *C. elegans*: extrachromosomal maintenance and integration of
940 transforming sequences. *EMBO J.* **10**, 3959–3970.
941 **Melo, J. A. and Ruvkun, G.** (2012). Inactivation of conserved *C. elegans* genes
942 engages pathogen- and xenobiotic-associated defenses. *Cell* **149**, 452–466.
943 **Mok, D. Z. L., Sternberg, P. W. and Inoue, T.** (2015). Morphologically defined sub-
944 stages of *C. elegans* vulval development in the fourth larval stage. *BMC Dev.*
945 *Biol.* 1–8.
946 **Moribe, H., Yochem, J., Yamada, H., Tabuse, Y., Fujimoto, T. and Mekada, E.**
947 (2004). Tetraspanin protein (TSP-15) is required for epidermal integrity in
948 *Caenorhabditis elegans*. *J. Cell Sci.* **117**, 5209–5220.
949 **Morse, D., Cermakian, N., Brancorsini, S., Parvinen, M. and Sassone-Corsi, P.**
950 (2003). No circadian rhythms in testis: Period1 expression is clock independent
951 and developmentally regulated in the mouse. *Mol. Endocrinol.* **17**, 141–151.
952 **Myllyharju, J. and Kivirikko, K. I.** (2004). Collagens, modifying enzymes and their
953 mutations in humans, flies and worms. *Trends Genet. TIG* **20**, 33–43.
954 **Nelson, F. K., Albert, P. S. and Riddle, D. L.** (1983). Fine structure of the
955 *Caenorhabditis elegans secretory-excretory system*. *J. Ultrastruct. Res.* **82**, 156–
956 171.

957 **Nonet, M. L.** (2020). Efficient Transgenesis in *Caenorhabditis elegans* Using Flp
958 Recombinase-Mediated Cassette Exchange. *Genetics* **215**, 903–921.
959 **Page, A. P. and Johnstone, I. L.** (2007). The cuticle. *WormBook.* 1–15.
960 **Paix, A., Wang, Y., Smith, H. E., Lee, C.-Y. S., Calidas, D., Lu, T., Smith, J.,**
961 **Schmidt, H., Krause, M. W. and Seydoux, G.** (2014). Scalable and versatile
962 genome editing using linear DNAs with microhomology to Cas9 Sites in
963 *Caenorhabditis elegans*. *Genetics* **198**, 1347–1356.
964 **Paix, A., Folkmann, A., Rasoloson, D. and Seydoux, G.** (2015). High Efficiency,
965 Homology-Directed Genome Editing in *Caenorhabditis elegans* Using CRISPR-
966 Cas9 Ribonucleoprotein Complexes. *Genetics* **201**, 47–54.
967 **Posch, A., Kohn, J., Oh, K., Hammond, M. and Liu, N.** (2013). V3 stain-free workflow
968 for a practical, convenient, and reliable total protein loading control in western
969 blotting. *J. Vis. Exp.* 50948.
970 **Pujol, N., Cypowyj, S., Ziegler, K., Millet, A., Astrain, A., Goncharov, A., Jin, Y.,**
971 **Chisholm, A. D. and Ewbank, J. J.** (2008). Distinct innate immune responses to
972 infection and wounding in the *C. elegans* epidermis. *Curr. Biol.* **18**, 481–489.
973 **R Core Team** *R: A language and environment for statistical computing.* Vienna,
974 Austria: R Foundation for Statistical Computing.
975 **Ragle, J. M., Aita, A. L., Morrison, K. N., Martinez-Mendez, R., Saeger, H. N.,**
976 **Ashley, G. A., Johnson, L. C., Schubert, K. A., Shakes, D. C. and Ward, J. D.**
977 (2020). The conserved molting/circadian rhythm regulator NHR-23/NR1F1 serves
978 as an essential co-regulator of *C. elegans* spermatogenesis. *Development* **147**,
979 dev193862.
980 **Roach, N. P., Sadowski, N., Alessi, A. F., Timp, W., Taylor, J. and Kim, J. K.** (2020).
981 The full-length transcriptome of *C. elegans* using direct RNA sequencing.
982 *Genome Res.*
983 **Ruaud, A.-F. and Bessereau, J.-L.** (2006). Activation of nicotinic receptors uncouples
984 a developmental timer from the molting timer in *C. elegans*. *Development* **133**,
985 2211–2222.
986 **Ruaud, A.-F., Lam, G. and Thummel, C. S.** (2010). The *Drosophila* nuclear receptors
987 DHR3 and FTZ-F1 control overlapping developmental responses in late

988 embryos. *Development* **137**, 123–131.
989 **Sandhu, A., Badal, D., Sheokand, R., Tyagi, S. and Singh, V.** (2021). Specific
990 collagens maintain the cuticle permeability barrier in *Caenorhabditis elegans*.
991 *Genetics* **217**,.
992 **Sapio, M. R., Hilliard, M. A., Cermola, M., Favre, R. and Bazzicalupo, P.** (2005). The
993 Zona Pellucida domain containing proteins, CUT-1, CUT-3 and CUT-5, play
994 essential roles in the development of the larval alae in *Caenorhabditis elegans*.
995 *Dev. Biol.* **282**, 231–245.
996 **Schindler, A. J., Baugh, L. R. and Sherwood, D. R.** (2014). Identification of Late
997 Larval Stage Developmental Checkpoints in *Caenorhabditis elegans* Regulated
998 by Insulin/IGF and Steroid Hormone Signaling Pathways. *PLoS Genet.* **10**,
999 e1004426.
1000 **Singh, R. N. and Sulston, J. E.** (1978). Some observations on molting in *C. elegans*.
1001 *Nematologica* **24**, 63–71.
1002 **Stempor, P. and Ahringer, J.** (2016). SeqPlots - Interactive software for exploratory
1003 data analyses, pattern discovery and visualization in genomics. *Wellcome Open*
1004 *Res.* **1**, 14.
1005 **Sulston, J. E. and Horvitz, H. R.** (1977). Post-embryonic cell lineages of the
1006 nematode, *Caenorhabditis elegans*. *Dev. Biol.* **56**, 110–156.
1007 **Tabara, H., Sarkissian, M., Kelly, W. G., Fleenor, J., Grishok, A., Timmons, L., Fire,**
1008 **A. and Mello, C. C.** (1999). The *rde-1* gene, RNA interference, and transposon
1009 silencing in *C. elegans*. *Cell* **99**, 123–132.
1010 **Taubert, S., Ward, J. D. and Yamamoto, K. R.** (2011). Nuclear hormone receptors in
1011 nematodes: Evolution and function. *Mol. Cell. Endocrinol.* **334**, 49–55.
1012 **Telford, M. J., Bourlat, S. J., Economou, A., Papillon, D. and Rota-Stabelli, O.**
1013 (2008). The evolution of the Ecdysozoa. *Philos. Trans. R. Soc. B Biol. Sci.* **363**,
1014 1529–1537.
1015 **Teuscher, A. C., Jongsma, E., Davis, M. N., Statzer, C., Gebauer, J. M., Naba, A.**
1016 **and Ewald, C. Y.** (2019). The *in-silico* characterization of the *Caenorhabditis*
1017 *elegans* matrisome and proposal of a novel collagen classification. *Matrix Biol.*
1018 *Plus* **1**, 100001.

1019 **Thummel, C. S.** (1990). Puffs and gene regulation-molecular insights into the
1020 *Drosophila* ecdysone regulatory hierarchy. *BioEssays News Rev. Mol. Cell. Dev.*
1021 *Biol.* **12**, 561–568.
1022 **Tsiairis, C. and Großhans, H.** (2021). Chapter Two - Gene expression oscillations in
1023 *C. elegans* underlie a new developmental clock. In *Current Topics in*
1024 *Developmental Biology* (ed. Jarriault, S.) and Podbilewicz, B.), pp. 19–43.
1025 Academic Press.
1026 **Vo, A. A., Levenson, M. T., Ragle, J. M. and Ward, J. D.** (2021). Efficient generation
1027 of a single-copy *eft-3p::TIR1::F2A:: BFP::AID*::NLS* allele in the *C. elegans*
1028 *ttTi5605* insertion site through recombination-mediated cassette exchange.
1029 *MicroPublication Biol.* **2021**, 10.17912/micropub.biology.000425.
1030 **Vogel, C. and Marcotte, E. M.** (2012). Insights into the regulation of protein abundance
1031 from proteomic and transcriptomic analyses. *Nat. Rev. Genet.* **13**, 227–232.
1032 **Vuong-Brender, T. T. K., Suman, S. K. and Labouesse, M.** (2017). The apical ECM
1033 preserves embryonic integrity and distributes mechanical stress during
1034 morphogenesis. *Development* **144**, 4336–4349.
1035 **Ward, J. D.** (2015a). Rapid and Precise Engineering of the *Caenorhabditis elegans*
1036 Genome with Lethal Mutation Co-Conversion and Inactivation of NHEJ Repair.
1037 *Genetics* **199**, 363–377.
1038 **Ward, J. D.** (2015b). Rendering the Intractable More Tractable: Tools from
1039 *Caenorhabditis elegans* Ripe for Import into Parasitic Nematodes. *Genetics* **201**,
1040 1279–1294.
1041 **Ward, J. D., Bojanala, N., Bernal, T., Ashrafi, K., Asahina, M. and Yamamoto, K. R.**
1042 (2013). Sumoylated NHR-25/NR5A Regulates Cell Fate during *C. elegans* Vulval
1043 Development. *PLoS Genet.* **9**, e1003992.
1044 **Ward, J. D., Mullaney, B., Schiller, B. J., He, L. D., Petnic, S. E., Couillault, C.,**
1045 **Pujol, N., Bernal, T. U., Van Gilst, M. R., Ashrafi, K., et al.** (2014). Defects in
1046 the *C. elegans* acyl-CoA Synthase, *acs-3*, and Nuclear Hormone Receptor, *nhr-*
1047 *25*, Cause Sensitivity to Distinct, but Overlapping Stresses. *PLoS ONE* **9**,
1048 e92552.
1049 **Watts, J. S., Harrison, H. F., Omi, S., Guenthers, Q., Dalelio, J., Pujol, N. and**

1050 **Watts, J. L.** (2020). New Strains for Tissue-Specific RNAi Studies in
1051 *Caenorhabditis elegans*. *G3* **10**, 4167–4176.
1052 **Zaslaver, A., Mayo, A. E., Rosenberg, R., Bashkin, P., Sberro, H., Tsalyuk, M.,**
1053 **Surette, M. G. and Alon, U.** (2004). Just-in-time transcription program in
1054 metabolic pathways. *Nat. Genet.* **36**, 486–491.
1055 **Zhang, L., Ward, J. D., Cheng, Z. and Dernburg, A. F.** (2015). The auxin-inducible
1056 degradation (AID) system enables versatile conditional protein depletion in *C.*
1057 *elegans*. *Development* **142**, 4374–4384.
1058 **Zugasti, O. and Ewbank, J. J.** (2009). Neuroimmune regulation of antimicrobial
1059 peptide expression by a noncanonical TGF-β signaling pathway in
1060 *Caenorhabditis elegans* epidermis. *Nat. Immunol.* **10**, 249–256.
1061
1062